Identification of correlated inter-residue interactions in protein complex based on the fragment molecular orbital method

Tanaka, Shigenori ; Watanabe, Chiduru ; Honma, Teruki ; Fukuzawa, Kaori ; Ohishi, Kazue ; Maruyama, Tadashi

(Citation)
Journal of Molecular Graphics and Modelling,100:107650

(Issue Date)
2020-11

(Resource Type)
journal article

(Version)
Accepted Manuscript

(URL)
https://hdl.handle.net/20.500.14094/90007506

Identification of correlated inter-residue interactions in protein complex based on the fragment molecular orbital method

Shigenori Tanaka

Graduate School of System Informatics, Department of Computational Science, Kobe University, 1-1 Rokkodai, Nada-ku, Kobe 657-8501, Japan

Chiduru Watanabe

Center for Biosystems Dynamics Research, RIKEN, 1-7-22 Suehiro-cho, Tsurumi-ku, Yokohama, Kanagawa 230-0045, Japan
& JST PRESTO, 4-1-8, Honcho, Kawaguchi, Saitama 332-0012 Japan

Teruki Honma

Center for Biosystems Dynamics Research, RIKEN, 1-7-22 Suehiro-cho, Tsurumi-ku, Yokohama, Kanagawa 230-0045, Japan

Kaori Fukuzawa

Department of Physical Chemistry, School of Pharmacy and Pharmaceutical Sciences, Hoshi University, 2-4-41 Ebara, Shinagawa, Tokyo 142-8501, Japan

Kazue Ohishi

Faculty of Engineering, Tokyo Polytechnic University, 1583, Iiyama, Atsugi, Kanagawa 243-0297, Japan

Tadashi Maruyama

Kitasato University, 1-15-1, Kitazato, Minami, Sagamihara, Kanagawa 252-0373, Japan

Abstract

A theoretical scheme to systematically describe correlated (network-like)

Email address: tanaka2@kobe-u.ac.jp; Fax:+81-78-803-6621 (Shigenori Tanaka)

interactions between molecular fragments is proposed within the framework of the fragment molecular orbital (FMO) method. The method is mathematically based on the singular value decomposition (SVD) of the inter-fragment interaction energy (IFIE) matrix obtained by the FMO calculation, and can be applied to a comprehensive description of protein-protein interactions in the context of molecular recognition. In the present study we apply the proposed method to a complex of measles virus hemagglutinin and human SLAM receptor, thus finding a usefulness for efficiently eliciting the correlated interactions among the amino-acid residues involved in the two proteins. Additionally, collective interaction networks by amino-acid residues important for mutation experiments can be clearly visualized.

Keywords: fragment molecular orbital method (FMO); inter-fragment interaction energy (IFIE); singular value decomposition (SVD); protein-protein interaction; measles virus (MV)

---

1. Introduction

Since its proposal in 1999 [1, 2], the fragment molecular orbital (FMO) method [3–5] has provided a powerful and useful tool to perform *ab initio* electronic-state calculations for biomolecular and other related systems. One of very advantageous features in the FMO method for biomolecular analyses is its ability to evaluate "effective interactions" between "fragments" that are usually chosen to be an amino-acid residue or a (small) ligand molecule as a unit component in protein-ligand complex system, for instance. This inter-fragment interaction is referred to as IFIE (Inter-Fragment Interaction Energy) or PIE (Pair Interaction Energy) in the literature [3–6], and plays a vital role in, *e.g.*, docking analysis by specifying important interactions involved in the object system. In fact, the FMO-IFIE analysis has been extensively applied to the investigations of mechanisms of molecular recognition associated with protein-protein [7–11], protein-nucleic acid [12–14], protein-drug [15–19], and other [20–25] intermolecular interactions.

In earlier studies, we applied the FMO-IFIE method to the analyses of intermolecular interactions of influenza virus hemagglutinin (HA) protein in complex with sialosaccharide receptors [23, 25] and Fab fragment of antibody [7, 8] for the investigation of mutation effects. Particularly, in the former analysis [25], we found an interesting phenomenon referred to as *indirect* effect in which the mutations of HA residues that do not strongly interact with the receptor significantly affect the change in binding affinity of complex, while the interactions between some unmutated residues in HA and the receptor often vary substantially due to the mutations at other residues. This unexpected effect has thus suggested a presence of correlated (network-like)

inter-fragment interactions, whose detailed mechanism has remained to be elucidated.

In biomolecular complex systems, the inter-fragment interactions are multiple in essence. Although the electron-correlated FMO-IFIE itself refers to an effective, renormalized interaction between single fragments in which some many-body effects are included, the total complex interactions should be described as a whole in terms of the set of all the IFIEs. In earlier investigations on protein-protein interaction (PPI) [10, 11], the network structure of IFIE (or PIE) was revealed in terms of the concept of Protein Residue Network (PRN). Concerning this issue of describing the correlated interactions due to multiple fragments, we have recently found a usefulness of the technique of singular value decomposition (SVD). In our previous study for protein-ligand systems [26], we applied the SVD for the calculated results of the IFIE matrix (amino-acid residues $\times$ various ligand compounds) to elicit the essential interactions and consequently improve the correlation between FMO results and experimental ligand (small compound) binding affinities. Through this method, we obtained the improved correlation with experimental results by extracting important singular eigenvectors that play essential roles for ligand binding.

In the present study we extend this SVD methodology to the description of protein-protein interaction (PPI) in order to comprehensively identify the correlated interactions among residues. By means of the SVD that enables a data compression similar to the principal component analysis (see Sec. 2.3), the network structure of IFIEs is systematically extracted. We here employ a complex system of measles virus hemagglutinin (MVH) and human SLAM

(signaling lymphocyte activation molecule) receptor as an example for the PPI analysis. Measles virus (MV) causes an acute and highly devastating contagious disease in humans. In a previous study [27], employing the crystal structures of three human receptors, SLAM, CD46, and Nectin-4, in complex with the measles virus hemagglutinin (MVH or HA), we computationally elucidated the details of binding energies between the amino-acid residues of HA and those of the receptors in terms of *ab initio* FMO method. The calculated IFIEs revealed a number of significantly interacting amino-acid residues of HA that played essential roles in binding to the receptors. As predicted from previously reported experiments, some important amino-acid residues of HA were shown to be common but others were specific to interactions with the three receptors. Further, we carried out FMO calculations for *in silico* experiments of amino-acid mutations, finding reasonable agreements with virological experiments concerning the substitution effect of residues. Thus, our study demonstrated that the electron-correlated FMO method is a powerful tool to exhaustively search for amino-acid residues that contribute to interactions with receptor molecules.

It is known that SLAM is the most important receptor for wild-type MV, because it is responsible for invasion and propagation, and also for pathogenesis in the infected animals [28]. Here, employing the IFIE matrix composed of the HA residues and the SLAM residues as the column and row elements, respectively, we assess the usefulness of the SVD analysis to comprehensively describe the PPIs. It is noted that we employ the result of FMO calculation *in vacuo* bacause the primary purpose of the present work is to propose a novel method and assess its validity, while the incorporation

of solvent effect is actually feasible in explicit or implicit way [29–31]. In the following section, we first illustrate the theoretical framework to obtain the correlated inter-fragment interactions in the FMO scheme. Test calculations employing a protein complex MVH-SLAM are carried out in Sec. 3, and their implications are discussed. Concluding remarks are given in Sec. 4.

2. Methods

2.1. Fragment molecular orbital (FMO) method and inter-fragment interaction energy (IFIE)

The FMO method [1–5] is a computational method that divides large molecules such as proteins into relatively small units called fragments, and then calculates the energy of the whole molecule and the electron density quantum-chemically by molecular orbital (MO) calculations of fragment monomers and fragment dimers (sometimes, trimers and tetramers are also considered [5]). By using this method, we can apply an *ab initio* MO method that has been shown to succeed for small compounds to macromolecules such as proteins without a significant loss in accuracy.

When dividing a large molecule into N_f fragments and letting the total electron energies of a fragment I and its pair IJ be E_I and E_{IJ}, respectively, the total electron energy of a molecule can be approximated (FMO2 approximation) as [3–5] :

$$E = \sum_{I>J} E_{IJ} - (N_f - 2) \sum_{I} E_I. \tag{1}$$

If $\Delta\mathbf{P}$ is the difference matrix of the electron density of monomer $(\mathbf{P}^I, \mathbf{P}^J)$ and dimer $(\mathbf{P}^{IJ})$, Eq. (1) can be transformed into the following equation:

$$E = \sum_{I>J}(E'_{IJ} - E'_I - E'_J) + \sum_{I>J}\mathrm{Tr}(\Delta\mathbf{P}^{IJ}\mathbf{V}^{IJ}) + \sum_I E'_I, \tag{2}$$

where $E'_I = E_I - V_I, E'_{IJ} = E_{IJ} - V_{IJ}, V_I = \mathrm{Tr}(\mathbf{P}^I\mathbf{V}^I)$ and $V_{IJ} = \mathrm{Tr}(\mathbf{P}^{IJ}\mathbf{V}^{IJ})$; V_I and V_{IJ} are the electrostatic potentials that fragment I and fragment pair IJ receive from surrounding fragments, respectively. We thus find

$$\Delta E_{IJ} = (E'_{IJ} - E'_I - E'_J) + \mathrm{Tr}(\Delta\mathbf{P}^{IJ}\mathbf{V}^{IJ}), \tag{3}$$

where ΔE_{IJ} can be interpreted as the interaction energy between the fragment pair of I and J. This ΔE_{IJ} is referred to as inter-fragment interaction energy (IFIE) [3–5].

In the FMO method, the interaction between amino-acid residues in protein complex can be identified as an IFIE. Then, the total or partial summation of IFIEs (namely, IFIE-sum) is an index representing the strength of the binding between a specific residue and a set of other residues. This notion of IFIE-sum has played a significant role in the FMO analysis on biomolecular recognition [5]. However, in the present study, we propose an alternative approach to systematically extracting the collective interactions among clustered residues, as detailed below.

2.2. Structure preparation

To analyze the molecular interactions between MVH and human SLAM, we retrieved the crystal structures of the complex (Fig. 1) from the Protein Data Bank (PDB entry: 3ALZ) for the FMO calculation. In this structure, the complex of MVH-SLAM was composed of HA monomer (Chain A) and one SLAM molecule (Chain B).

In the present study, molecular interactions were analyzed [27] by the FMO method with electron-correlated MP2/6-31G* scheme using the software ABINIT-MP [5]. The preparation of the complex structure used for FMO calculation was carried out through molecular modeling by the Molecular Operating Environment (MOE, CCG Inc.) [32]. After complementation of missing atoms (for capping the missing residues) and addition of hydrogen atoms, the positions of the added atoms were energetically optimized with the AMBER force field [32]. The inter-fragment interaction energies (IFIEs) [3–5] which are obtained as effective interactions between fragments (residues) in the quantum-chemical FMO calculations then provide useful information about the important amino-acid pairs between MVH and the SLAM receptor. For example, the negative value of IFIE indicates an attractive interaction between the two fragments representing an amino acid pair. The summation of all the IFIEs between residue pairs of MVH and SLAM receptor gives the binding energy [5].

2.3. Singular value decomposition (SVD)

An $m \times n$ matrix S with m and n-dimensional vectors as columns and rows can be related to an $m \times n$ diagonal matrix Σ that satisfies the following equation:

$$\Sigma = U^T S V. \tag{4}$$

Here, U is an $m \times m$ orthogonal matrix, and V is an $n \times n$ orthogonal matrix. If U and V are chosen appropriately, a pair of matrices can be made with Σ satisfying the condition described below. When it is rewritten, the following equation is obtained:

$$S = U\Sigma V^T. \tag{5}$$

This type of decomposition is called Singular Value Decomposition (SVD) [33–36]. For simplicity of description, we assume $m \geq n$. Otherwise, we can think of the transposed matrix S^T of S.

If σ_{ij} is an element of Σ, in the case of $i \neq j$, $\sigma_{ij} = 0$; in the case of $i = j$, for $1 \leq i \leq n$, $\sigma_{ij} = \sigma_i \geq 0$. At this time, $\sigma_1 \geq \sigma_2 \geq \sigma_3 \geq ...$, where σ_i is called a singular value of S, a column vector of U is a left singular vector, and a row of V^T is a right singular vector [33–36].

When the original matrix S is $m \times n$, the size of each matrix is the following; $S : m \times n$, $U : m \times m$, $\Sigma : m \times n$, and $V^T : n \times n$. When we consider a complex of protein A with m residues and protein B with n residues, the column vector of U is an orthonormal basis for each amino-acid residue in protein A and the row vector of V^T is an orthonormal basis for each amino-acid residue in protein B, where each singular vector has an independent meaning. In this paper, we analyze the singular vectors of U and V^T, and call them singular vectors 1, singular vectors 2, ... and so forth in order according to the associated singular values. To execute the singular value decompositions, we have used *numpy.linalg.svd* in NumPy (www.numpy.org).

In this way, through the application of SVD to the IFIE matrix S for protein complex, we can extract the correlated inter-residue interactions specified as singular components.

3. Results and discussion

3.1. SVD component analysis based on IFIEs

Through the FMO calculation for MVH-SLAM complex [27], we obtained an IFIE matrix composed of the residue components of MVH and those of SLAM, where $m = 416$ and $n = 110$ fragments were considered for MVH and SLAM, respectively. (The numbers of amino-acid residues contained in MVH and SLAM were 421 and 111, respectively, in which the disulfide bonds were divided.) Then, performing the SVD for the IFIE matrix, we have obtained the singular vectors for MVH and SLAM each with the corresponding singular values, which represent the modes of collective interaction pattern. The singular vectors 1-10 for MVH (HA) and SLAM are depicted in Fig. 2 and they are represented by color on the binding interface of the complex in Fig. 3. In particular, the first singular vectors of HA and SLAM are depicted in Fig. 4 for the complex form, thus showing particularly important interactions for complex formation. It is noted that the signs of the components of singular vectors do not necessarily correspond to those of the electric charges or the interaction energies associated with the amino-acid residues, due to the arbitrariness of the total phase (positive/negative) of the singular vectors.

As seen in Figs. 2-4, we can detect D505, D507, D530 and R533 on the HA side as important residues, which corresponds well to experimental findings [37–39]. On the other hand, we observe important residues of E75, K77 and E123 on the SLAM side, as was remarked in the previous study [27]. For singular vectors of top five rank 1-5 with higher singular values, the main components are predominantly composed of charged residues, showing the importance of electrostatic interactions especially in the case of MVH-SLAM

complex [27]. It is also noted that the interaction patterns given by each component of singular vectors 1-5 vary slightly but distinctively, thus showing their proper meanings. For the first singular vectors, we observe the tendency that the positively and negatively charged residues have the opposite signs and interact with the opposite-sign partners at the MVH-SLAM interface (Fig. 4). Interestingly, the relative phase (positive versus negative signs) of the dominant components is different between the singular vectors of 2 and 3, while the similar residues (*e.g.*, K77, E123, D505, D507 and R533) are involved, thus representing the complex mixture of attractive and repulsive interactions among charged residues. As for the rank 6-10 singular vectors, on the other hand, we find important contributions from neutral (polar and hydrophobic) residues, some of which are related to the hydrogen bond or dispersion interactions. In addition to the interactions associated with polar residues such as Ser and Thr, we observe those by Tyr, Phe, Leu and Ile in the eigenvectors 6-10. These charged and neutral residues significantly affect the binding affinity of MVH-SLAM complex when they are mutated [27].

A novel feature of the SVD methodology proposed in the present work is to explicitly elicit the correlated or cooperative IFIEs shared among multiple residue fragments. For example, as seen in Fig. 4, the cluster formed by E503, D505, D507 and R533 in HA and that by E75, K77, R90 and E123 in SLAM cooperatively interact with each other, thus yielding a collective interaction network for the formation of protein complex. Such a novel viewpoint would be essential when we describe the *indirect* interactions between fragments [25] as well as their direct interactions, which often play an important role in biomolecular complex formation but was difficult to detect by earlier analyses

[27] based on the individual IFIE values for each residue pair. Thus, the present approach can provide a novel FMO-based tool for the PPI analysis as an alternative to the earlier attempts based on other viewpoints such as the 3D Scattered Pair Interaction Energies (3D-SPIEs) [9] and the PIE-PRN [10, 11].

3.2. Effects of protonation state of His536

In some virological mutagenesis experiments, the importance of H536 residue in MVH on protein binding to SLAM was remarked [37–39]. However, in Figs. 2-4 above, we cannot detect the important contribution by H536 in the FMO calculation as well as in the earlier analysis [27]. One possibile reason for the disagreement with experiments may be concerned with the protonation state of His536. Therefore, we have also performed the FMO calculation and subsequent SVD analysis on MVH-SLAM complex in which the protonated (positively charged) His, Hip536, was used instead of the unprotonated (neutral) His, Hie536, employed in the calculation above. The first singular vector components obtained in this case are depicted in Figs. 5 and 6, which have revealed the importance of Hip536 in the interaction between HA and SLAM in marked contrast to the case with Hie536. The calculated results for the rank 1-10 singular vectors for HA and SLAM are depicted in Figs. S1 and S2 in the Supplementary data. Thus, we should keep in mind the possibility that the protonation state of H536 may be varied due to some reasons such as those changes of surrounding environments associated with pH, ionic strength, charged states of other residues and structural change.

3.3. SCIFIE analysis

It is well known that the FMO calculations performed *in vacuo* give the IFIE values that overestimate the electrostatic interactions at the far distances [5]. Although we may take explicit or implicit account of solvation effects [29–31] to overcome this difficulty, we here resort to a post-FMO processing scheme called Statistically Corrected IFIE (SCIFIE) [40] by which the effective screening (electrostatic shielding) in the long range is partially performed. The results for the singular vectors of top 10 rank for HA and SLAM are shown in Figs. S3 and S4 in the Supplementary data for the cases of Hie536 and Hip536, respectively. We also give the comparison of the first singular vectors obtained through IFIE with Hie536, IFIE with Hip536, SCIFIE with Hie536 and SCIFIE with Hip536 in Fig. 7. As seen in these figures, the SCIFIE protocol relevantly remedies the screening (electrostatic shielding) issue by erasing the redundant long-range interaction components in protein complex. Figure 8 clearly illustrates this point in terms of comparison between the IFIE and SCIFIE results for the first singular vectors, in which the long-range contributions are reduced without the significant influence on the interactions at the binding interface. Finally, we show in Table 1 the comparison of the contributions from each singular value component in all the four cases of IFIE with Hie536, IFIE with Hip536, SCIFIE with Hie536 and SCIFIE with Hip536. It is thus observed that the SVD contributions up to the 10th component give more than 83% occupancy in the total sum, dominating the MVH-SLAM interactions. In this way, the present compression scheme for the original IFIE data would provide a computational basis to efficiently describe PPIs.

4. Concluding remarks

In this study, we have proposed a novel methodology to efficiently obtain and visualize the correlated inter-fragment interactions in the FMO calculations for protein complex. With the aid of the SVD technique for the efficient data compression, the IFIE matrix composed of the residue components from each protein can be decomposed into the contributions from individual singular-value components that comprehensively describe the cooperative interaction network among amino-acid residues. We have applied this method to the analysis of molecular recognition between the measles virus HA and its SLAM receptor to assess its feasibility and usefulness. Collective interaction patterns formed by some important residues, which could not be described in earlier FMO-IFIE studies based on individual fragment interactions, were thus identified in agreement with experimental observations. In addition, the significances of the protonation state of His536 and of the electrostatic screening effect were addressed in the present study, while the explicit or implicit inclusion of the solvation effects would be an important issue [29–31] in actual pharmaceutical applications. For the future development, the incorporation of the pair interaction energy decomposition analysis (PIEDA) [41] would be interesting to discriminate the contributions from various kinds of molecular interactions. The proposed method would also be applicable to the analysis of molecular recognition associated with the new coronavirus SARS-CoV-2, *e.g.*, for a complex between the spike protein and the angiotensin-converting enzyme 2 (ACE2) [42, 43].

Acknowledgements

S.T. would like to acknowledge the Grants-in-Aid for Scientific Research (Nos. 17H06353 and 18K03825) from the Ministry of Education, Cultute, Sports, Science and Technology (MEXT), Japan. C.W. acknowledges the JST PRESTO Grant Number JPMJPR18GD, Japan. This research was performed in the activities of the FMO drug design consortium (FMODD).

Appendix A. Supplementary data

Figures S1-S4 are given with their legends in the Supplementary data.

References

[1] K. Kitaura, E. Ikeo, T. Asada, T. Nakano, M. Uebayasi, Chem. Phys. Lett. 313 (1999) 701.

[2] T. Nakano, T. Kaminuma, T. Sato, Y. Akiyama, M. Uebayashi, K. Kitaura, Chem. Phys. Lett. 318 (2000) 614.

[3] D.G. Fedorov, K. Kitaura, in Modern Methods for Theoretical Physical Chemistry of Biopolymers, ed. E.B. Starikov, J.P. Lewis, S. Tanaka, Elsevier, Amsterdam, 2006, p. 3-38.

[4] D.G. Fedorov, K. Kitaura, The Fragment Molecular Orbital Method: Practical Applications to Large Molecular Systems, CRC Press, Boca Raton, FL, 2009.

[5] S. Tanaka, Y. Mochizuki, Y. Komeji, Y. Okiyama, K. Fukuzawa, Phys. Chem. Chem. Phys. 16 (2014) 10310.

[6] I. Kurisaki, K. Fukuzawa, Y. Komeiji, Y. Mochizuki, T. Nakano, J. Imada, A. Chmielewski, S.M. Rothstein, H. Watanabe, S. Tanaka, Biophys. Chem. 130 (2007) 1.

[7] K. Takematsu, K. Fukuzawa, K. Omagari, S. Nakajima, K. Nakajima, Y. Mochizuki, T. Nakano, H. Watanabe, S. Tanaka, J. Phys. Chem. B 113 (2009) 4991.

[8] A. Yoshioka, K. Fukuzawa, Y. Mochizuki, K. Yamashita, T. Nakano, Y. Okiyama, E. Nobusawa, K. Nakajima, S. Tanaka, J. Mol. Graph. Model. 30 (2011) 110.

[9] H. Lim, J. Chun, X. Jin, J. Kim, J.H. Yoon, K.T. No, Sci. Rep. 9 (2019) 16727.

[10] A. Heifetz, I. Morao, M.M. Babu, T. James, M.W.Y. Southey, D.G. Fedorov, M. Aldeghi, M.J. Bodkin, A. Townsend-Nicholson, J. Chem. Theory Comput. 16 (2020) 2814.

[11] A. Heifetz, V. Sladek, A. Townsend-Nicholson, D.G. Fedorov, Methods Mol. Biol. 2114 (2020) 187.

[12] K. Fukuzawa, Y. Komeiji, Y. Mochizuki, T. Nakano, S. Tanaka, J. Comput. Chem. 27 (2006) 948.

[13] I. Kurisaki, K. Fukuzawa, T. Nakano, Y. Mochizuki, H. Watanabe, S. Tanaka, J. Mol. Struct. THEOCHEM 962 (2010) 45.

[14] H. Mori, K. Ueno-Noto, J. Phys. Chem. B 115 (2011) 4774.

[15] I. Nakanishi, D.G. Fedorov, K. Kitaura, Proteins 68 (2007) 145.

[16] T. Ozawa, E. Tsuji, M. Ozawa, C. Handa, H. Mukaiyama, T. Nishimura, S. Kobayashi, K. Okazaki, Bioorg. Med. Chem. 16 (2008) 10311.

[17] T. Ishikawa, T. Ishikura, K. Kuwata, J. Comput. Chem. 30 (2009) 2594.

[18] T. Yoshida, Y. Munei, S. Hitaoka, H. Chuman, J. Chem. Inf. Model. 50 (2010) 850.

[19] O. Ichihara, J. Barker, R.J. Law, M. Whittaker, Mol. Inf. 30 (2011) 298.

[20] K. Fukuzawa, Y. Mochizuki, S. Tanaka, K. Kitaura, T. Nakano, J. Phys. Chem. B 110 (2006) 16102.

[21] M. Ito, K. Fukuzawa, Y. Mochizuki, T. Nakano, S. Tanaka, J. Phys. Chem. A 112 (2008) 1986.

[22] H. Watanabe, T. Enomoto, S. Tanaka, Biochem. Biophys. Res. Commun. 361 (2007) 367.

[23] T. Iwata, K. Fukuzawa, K. Nakajima, S. Aida-Hyugaji, Y. Mochizuki, H. Watanabe, S. Tanaka, Comput. Biol. Chem. 32 (2008) 198.

[24] A. Tagami, N. Ishibashi, D. Kato, N. Taguchi, Y. Mochizuki, H. Watanabe, M. Ito, S. Tanaka, Chem. Phys. Lett. 472 (2009) 118.

[25] S. Anzaki, C. Watanabe, K. Fukuzawa, Y. Mochizuki, S. Tanaka, J. Mol. Graph. Model. 53 (2014) 48.

[26] K. Maruyama, Y. Sheng, H. Watanabe, K. Fukuzawa, S. Tanaka, Comput. Theor. Chem. 1132 (2018) 23.

[27] F. Xu, S. Tanaka, H. Watanabe, Y. Shimane, M. Iwasawa, K. Ohishi, T. Maruyama, Viruses 10 (2018) 236.

[28] V.H. Leonard, G. Hodge, J. ReysDel Valle, M.B. McChesney, R. Cattaneo, J. Virol. 84 (2010) 3413.

[29] Y. Okiyama, T. Nakano, C. Watanabe, K. Fukuzawa, Y. Mochizuki, S. Tanaka, J. Phys. Chem. B 122 (2018) 4457.

[30] Y. Okiyama, C. Watanabe, K. Fukuzawa, Y. Mochizuki, T. Nakano, S. Tanaka, J. Phys. Chem. B 123 (2019) 957.

[31] Y. Okiyama, K. Fukuzawa, Y. Komeiji, S. Tanaka, Methods Mol. Biol. 2114 (2020) 105.

[32] Molecular Operating Environment (MOE). Chemical Computing Group (CCG) Inc., Montreal, QC, Canada, 2016.

[33] V. Klema, A.Laud, IEEE Trans. Automat. Contr. 25 (1980) 164.

[34] F. Kleibergen, R. Paap, J. Economet. 133 (2006) 97.

[35] M. Brand, Linear Algebra Appl. 415 (2006) 20.

[36] L. De Lathauwer, B. De Moor, J. Vandewalle, SIAM J. Mat. Anal. 21 (2000) 1253.

[37] S. Vongpunsawad, N. Oezgun, W. Braun, R. Cattaneo, J. Virol. 78 (2004) 302.

[38] N. Masse, M. Ainouze, B. Neel, T.F. Wild, R. Buckland, J.P.M. Langedijk, J. Virol. 78 (2004) 9051.

[39] C.K. Navaratnarajah, S. Vongpunsawad, N. Oezguen, T. Stehle, W. Braun, T. Hashiguchi, K. Maenaka, Y. Yanagi, R. Cattaneo, J. Biol. Chem. 283 (2008) 11763.

[40] S. Tanaka, C. Watanabe, Y. Okiyama, Chem. Phys. Lett. 556 (2013) 272.

[41] D.G. Fedorov, K. Kitaura, J. Comput. Chem. 28 (2007) 222.

[42] D. Wrapp, N. Wang, K.S. Corbett, J.A. Goldsmith, C.-L. Hsieh, O. Abiona, B.S. Graham, J.S. McLellan, Science 10.1126/science.abb2507 (2020).

[43] R. Yan, Y. Zhang, Y. Li, L. Xia, Y. Guo, Q. Zhou, Science 10.1126/science.abb2762 (2020).

Figure and table captions

Figure 1: Complex structure of MVH (measles virus HA) and human SLAM (PDB code: 3ALZ).

Figure 2: Singular vectors 1-10 with decreasing singular values for SLAM (left, V_1-V_{10}) and HA (right, U_1-U_{10}). The abscissa refers to the amino-acid numbers and the ordinate represents the values of singular vector components normalized by the maximum value. The IFIE values were obtained by the FMO calculation in which Hie536 (an unprotonated form of His536) was employed.

Figure 3: Residues with large magnitude in each singular vector 1-10 for SLAM (left) and HA (right). The IFIE values used for the SVD analysis were the same as those in Fig. 2. Blue and red colors indicate positive and negative values, respectively, whose deepness of the hue refers to the normalized magnitude.

Figure 4: (A) Residues with large magnitude in the first singular vector 1 for the complex of HA (right) and SLAM (left). The IFIE values used for the SVD analysis were the same as those in Fig. 2. Blue and red colors indicate positive and negative values, respectively, whose deepness of the hue refers to the magnitude. The suffixes "H" and "S" indicate the residues of HA and SLAM, respectively. The position of H536 (Hie536) is highlighted by the yellow dotted circle. (B) Interaction surfaces of HA (right) and SLAM (left) depicted by opening out the interfaces of the complex with 90° rotation. (C) Interacting residues of the target molecules depicted by the ball-and-stick

representation on the surface of partner proteins.

Figure 5: (A) Residues with large magnitude in the first singular vector 1 for the complex of HA (right) and SLAM (left), where the IFIE values were obtained by the FMO calculation in which Hip536 was employed. Blue and red colors indicate positive and negative values, respectively, whose deepness of the hue refers to the magnitude. The suffixes "H" and "S" indicate the residues of HA and SLAM, respectively. The position of H536 (Hip536) is highlighted by the yellow dotted circle. (B) Interaction surfaces of HA (right) and SLAM (left) depicted by opening out the interfaces of the complex with 90° rotation. (C) Interacting residues of the target molecules depicted by the ball-and-stick representation on the surface of partner proteins.

Figure 6: First singular vectors for SLAM (left, V_1) and HA (right, U_1), where the IFIE values for the SVD analysis were obtained by the FMO calculation in which Hip536 was employed. The abscissa refers to the amino-acid numbers and the ordinate represents the values of singular vector components normalized by the maximum value.

Figure 7: Comparison among the first singular vectors for SLAM (left) and HA (right) obtained in terms of SVD analyses on (A) IFIE with Hie536, (B) IFIE with Hip536, (C) SCIFIE with Hie536 and (D) SCIFIE with Hip536. The abscissa refers to the amino-acid numbers and the ordinate represents the values of singular vector components normalized by the maximum value.

Figure 8: Comparison between the first singular vectors for the IFIE with Hie536 (A-C) and the SCIFIE with Hie536 (D-F). HA and SLAM are located

on the right and left hand sides in each complex, respectively, and blue and red colors refer to the positive and negative values of each residue component, respectively, with their deepness of the hue representing the magnitude. (B)-(C) and (E)-(F) refer to the normalized values on the SLAM-HA interface in the cases of IFIE and SCIFIE, respectively.

Table 1: Comparison of top 10 singular values among the results for IFIE with Hie536, IFIE with Hip536, SCIFIE with Hie536, and SCIFIE with Hip536. Their contribution fractions and the accumulated occupancies are also shown.

Figure. 1

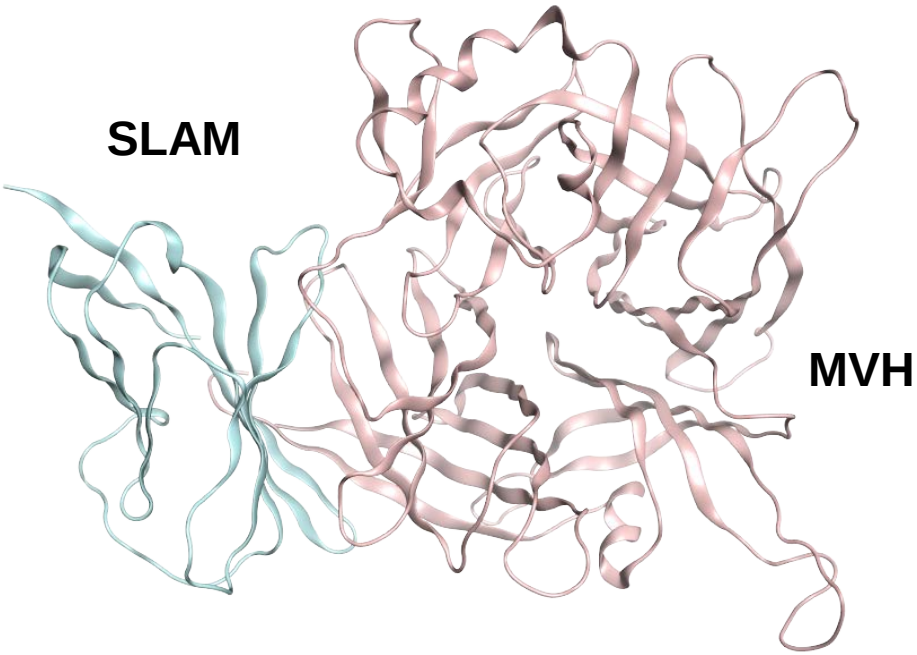

Figure 2

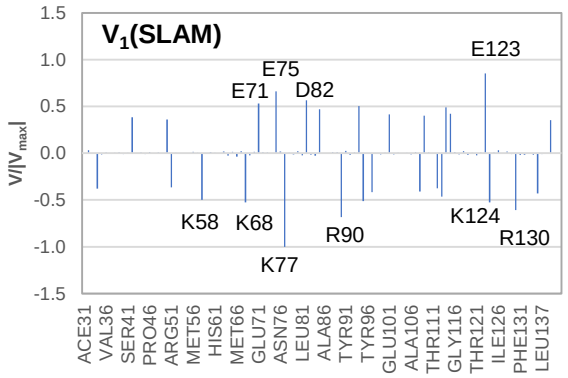
V1(SLAM)
E123
E75
E71
D82
K58
K68
K77
R90
K124
R130
V/|Vmax|
ACE31 VAL36 SER41 PRO46 ARG51 MET56 HIS61 MET66 GLU71 ASN76 LEU81 ALA86 TYR91 TYR96 GLU101 ALA106 THR111 GLY116 THR121 ILE126 PHE131 LEU137

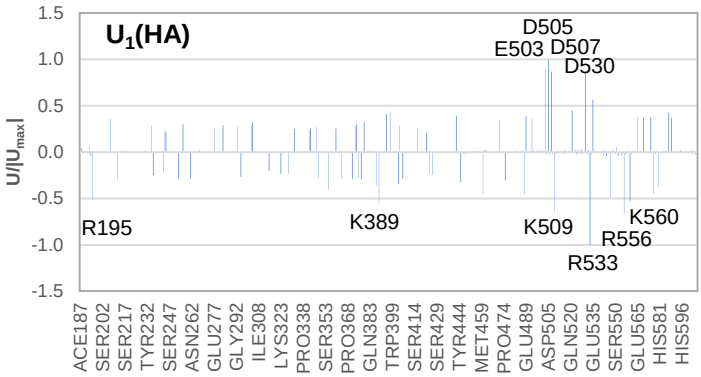
U1(HA)
D505
E503 D507
D530
R195
K389
K509
K560
R556
R533
U/|Umax|
ACE187 SER202 SER217 TYR232 SER247 ASN262 GLU277 GLY292 ILE308 LYS323 PRO338 SER353 PRO368 GLN383 TRP399 SER414 SER429 TYR444 MET459 PRO474 GLU489 ASP505 GLN520 GLU535 SER550 GLU565 HIS581 HIS596

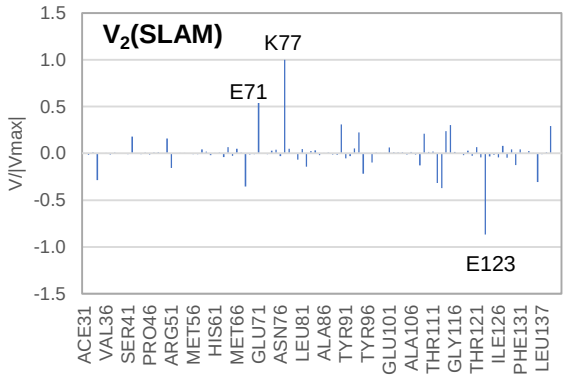
V2(SLAM)
K77
E71
E123
V/|Vmax|
ACE31 VAL36 SER41 PRO46 ARG51 MET56 HIS61 MET66 GLU71 ASN76 LEU81 ALA86 TYR91 TYR96 GLU101 ALA106 THR111 GLY116 THR121 ILE126 PHE131 LEU137

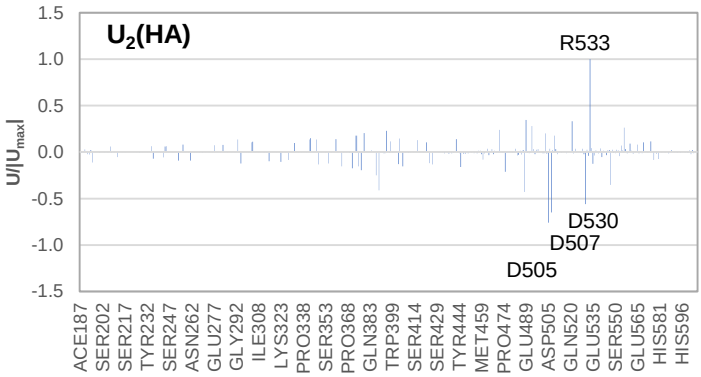
U2(HA)
R533
D530
D507
D505
U/|Umax|
ACE187 SER202 SER217 TYR232 SER247 ASN262 GLU277 GLY292 ILE308 LYS323 PRO338 SER353 PRO368 GLN383 TRP399 SER414 SER429 TYR444 MET459 PRO474 GLU489 ASP505 GLN520 GLU535 SER550 GLU565 HIS581 HIS596

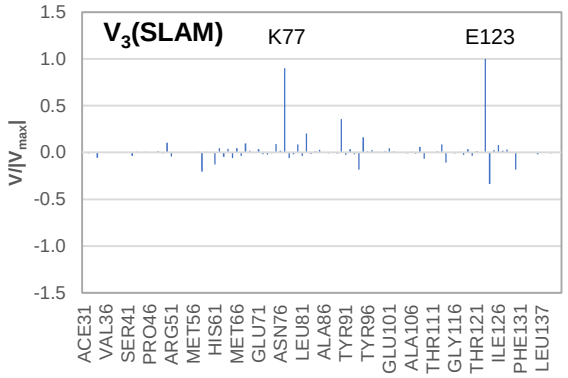
V3(SLAM)
K77
E123
V/|Vmax|
ACE31 VAL36 SER41 PRO46 ARG51 MET56 HIS61 MET66 GLU71 ASN76 LEU81 ALA86 TYR91 TYR96 GLU101 ALA106 THR111 GLY116 THR121 ILE126 PHE131 LEU137

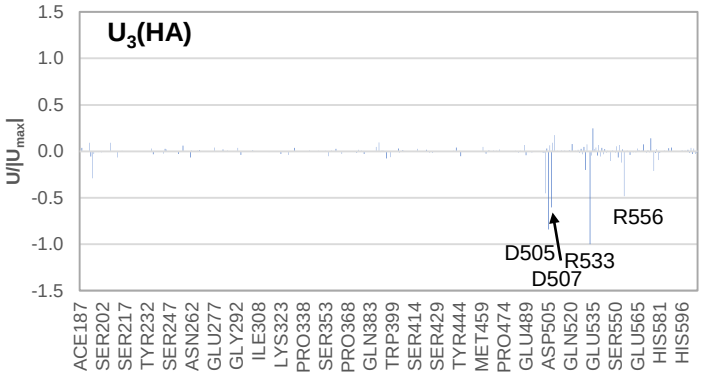
U3(HA)
R556
D505
R533
D507
U/|Umax|
ACE187 SER202 SER217 TYR232 SER247 ASN262 GLU277 GLY292 ILE308 LYS323 PRO338 SER353 PRO368 GLN383 TRP399 SER414 SER429 TYR444 MET459 PRO474 GLU489 ASP505 GLN520 GLU535 SER550 GLU565 HIS581 HIS596

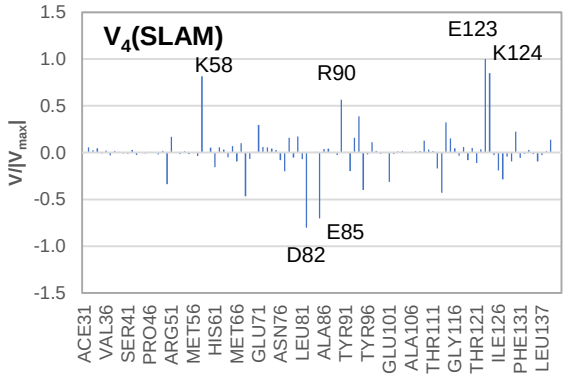
V4(SLAM)
E123
K124
K58
R90
E85
D82
V/|Vmax|
ACE31 VAL36 SER41 PRO46 ARG51 MET56 HIS61 MET66 GLU71 ASN76 LEU81 ALA86 TYR91 TYR96 GLU101 ALA106 THR111 GLY116 THR121 ILE126 PHE131 LEU137

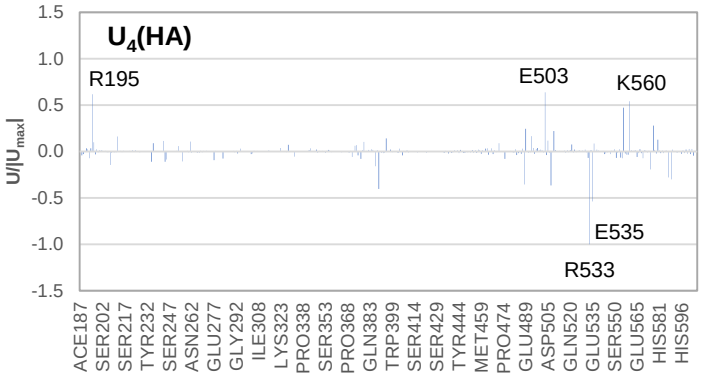
U4(HA)
R195
E503
K560
E535
R533
U/|Umax|
ACE187 SER202 SER217 TYR232 SER247 ASN262 GLU277 GLY292 ILE308 LYS323 PRO338 SER353 PRO368 GLN383 TRP399 SER414 SER429 TYR444 MET459 PRO474 GLU489 ASP505 GLN520 GLU535 SER550 GLU565 HIS581 HIS596

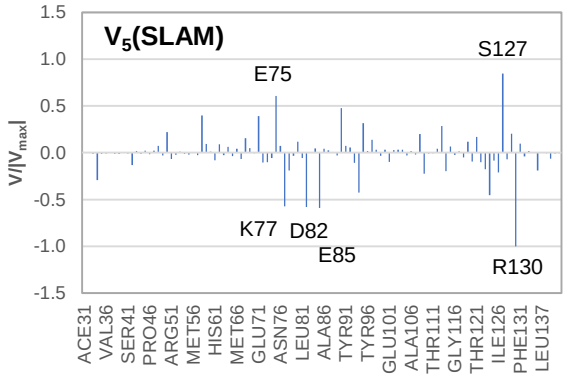
V5(SLAM)
S127
E75
K77
D82
E85
R130
V/|Vmax|
ACE31 VAL36 SER41 PRO46 ARG51 MET56 HIS61 MET66 GLU71 ASN76 LEU81 ALA86 TYR91 TYR96 GLU101 ALA106 THR111 GLY116 THR121 ILE126 PHE131 LEU137

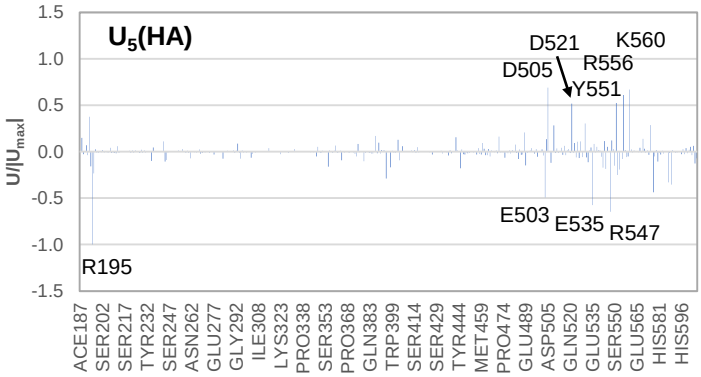
U5(HA)
D521
K560
D505
R556
Y551
E503
E535
R547
R195
U/|Umax|
ACE187 SER202 SER217 TYR232 SER247 ASN262 GLU277 GLY292 ILE308 LYS323 PRO338 SER353 PRO368 GLN383 TRP399 SER414 SER429 TYR444 MET459 PRO474 GLU489 ASP505 GLN520 GLU535 SER550 GLU565 HIS581 HIS596

Figure. 2 (continued)

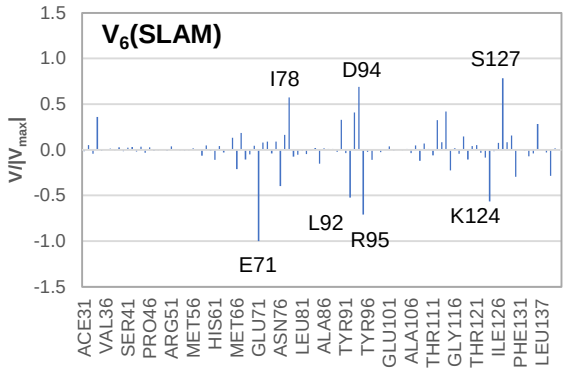

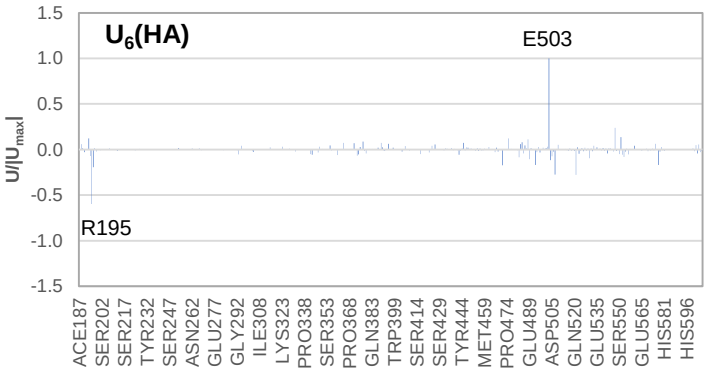

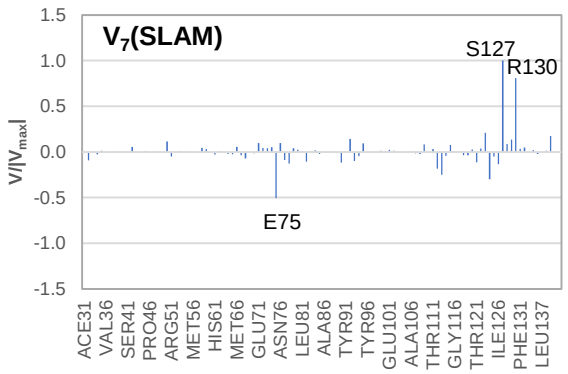

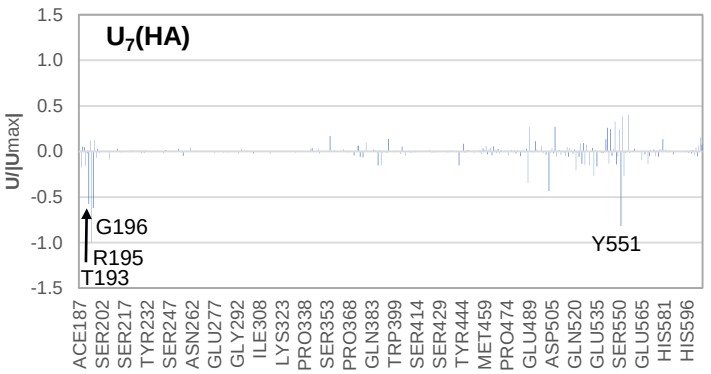

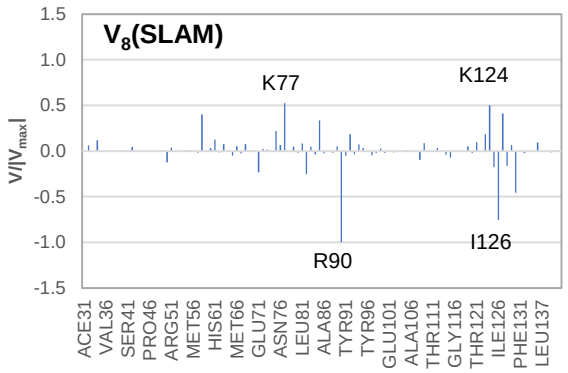

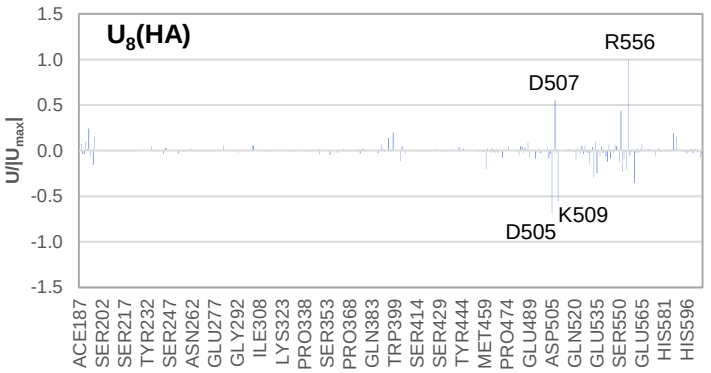

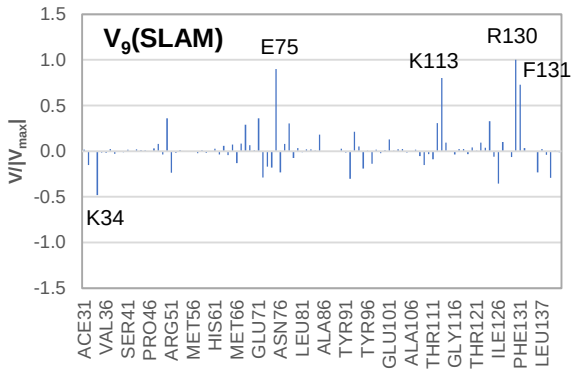

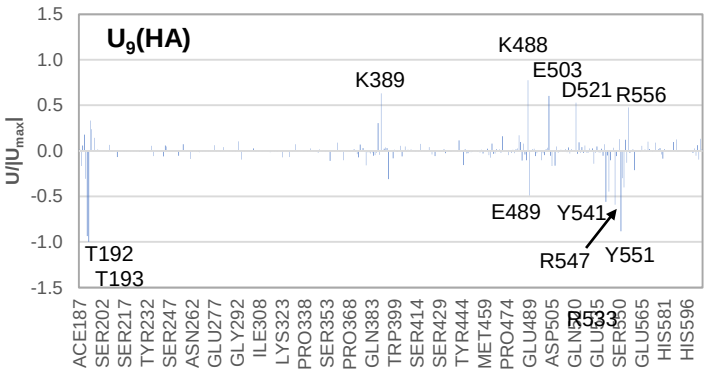

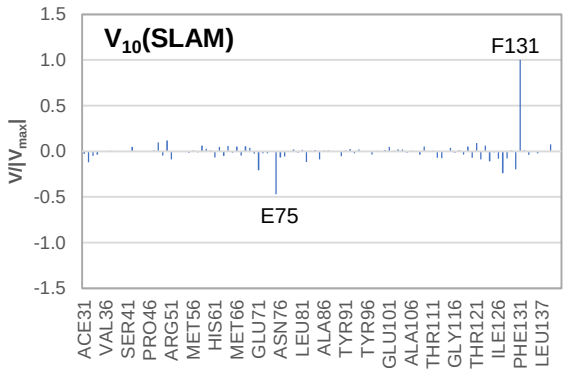

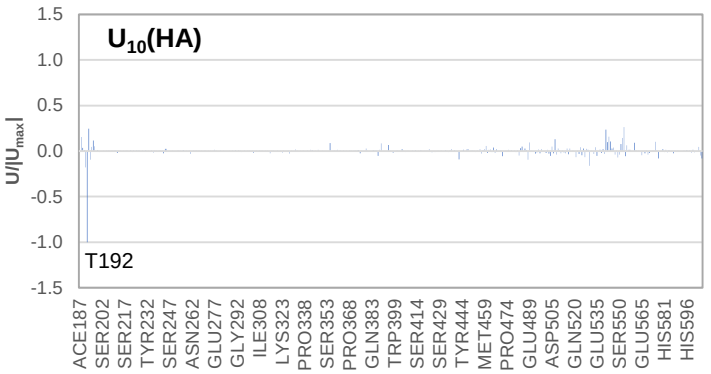

Figure. 3

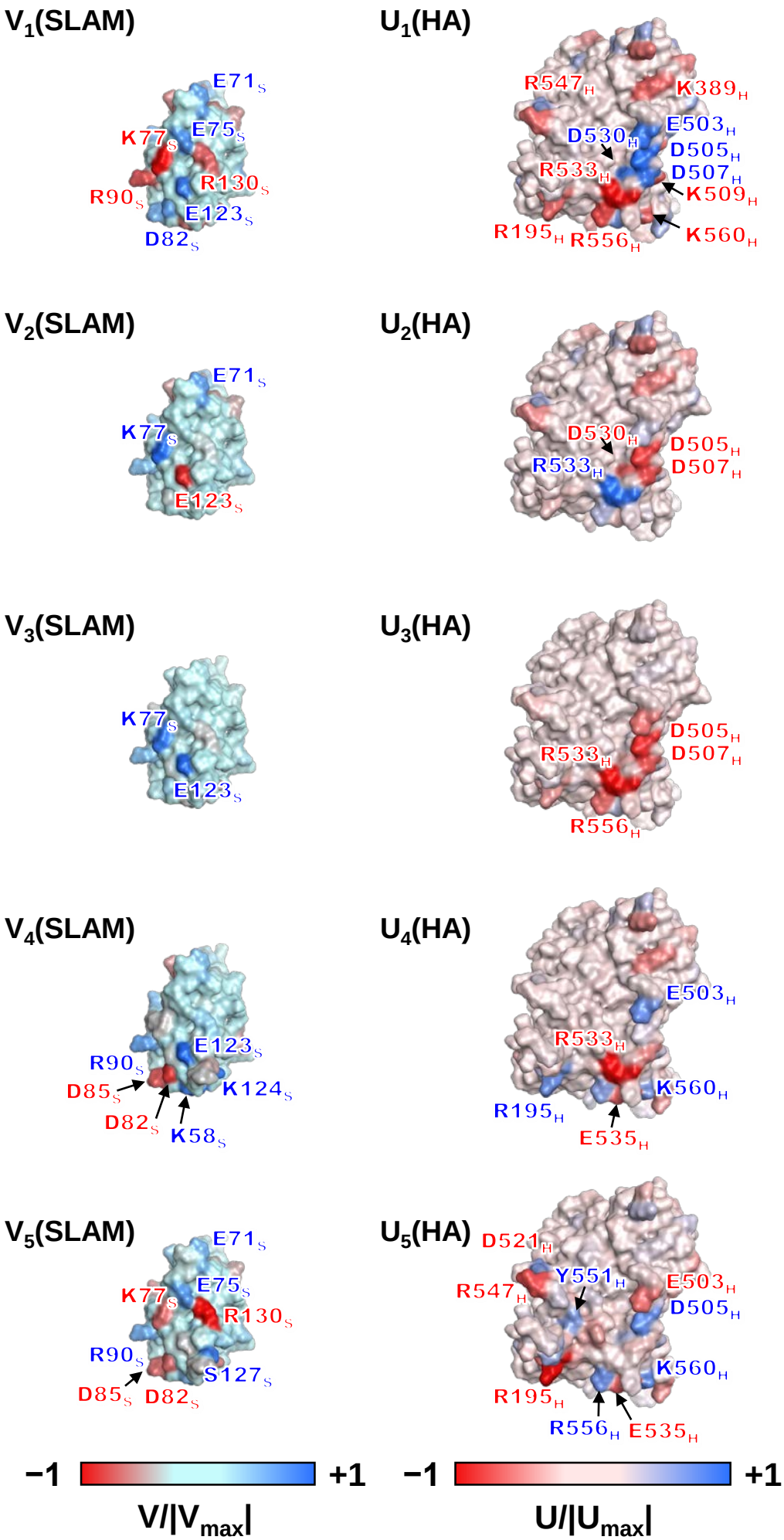
V1(SLAM)
E71S
K77S
E75S
R130S
R90S
E123S
D82S
U1(HA)
R547H
K389H
E503H
D530H
D505H
R533H
D507H
K509H
R195H
R556H
K560H
V2(SLAM)
E71S
K77S
E123S
U2(HA)
D530H
D505H
R533H
D507H
V3(SLAM)
K77S
E123S
U3(HA)
D505H
R533H
D507H
R556H
V4(SLAM)
E123S
R90S
D85S
K124S
D82S
K58S
U4(HA)
E503H
R533H
K560H
R195H
E535H
V5(SLAM)
E71S
K77S
E75S
R130S
R90S
S127S
D85S
D82S
U5(HA)
D521H
Y551H
R547H
E503H
D505H
K560H
R195H
R556H
E535H
−1
+1
V/|Vmax|
−1
+1
U/|Umax|

Figure. 3 (continued)

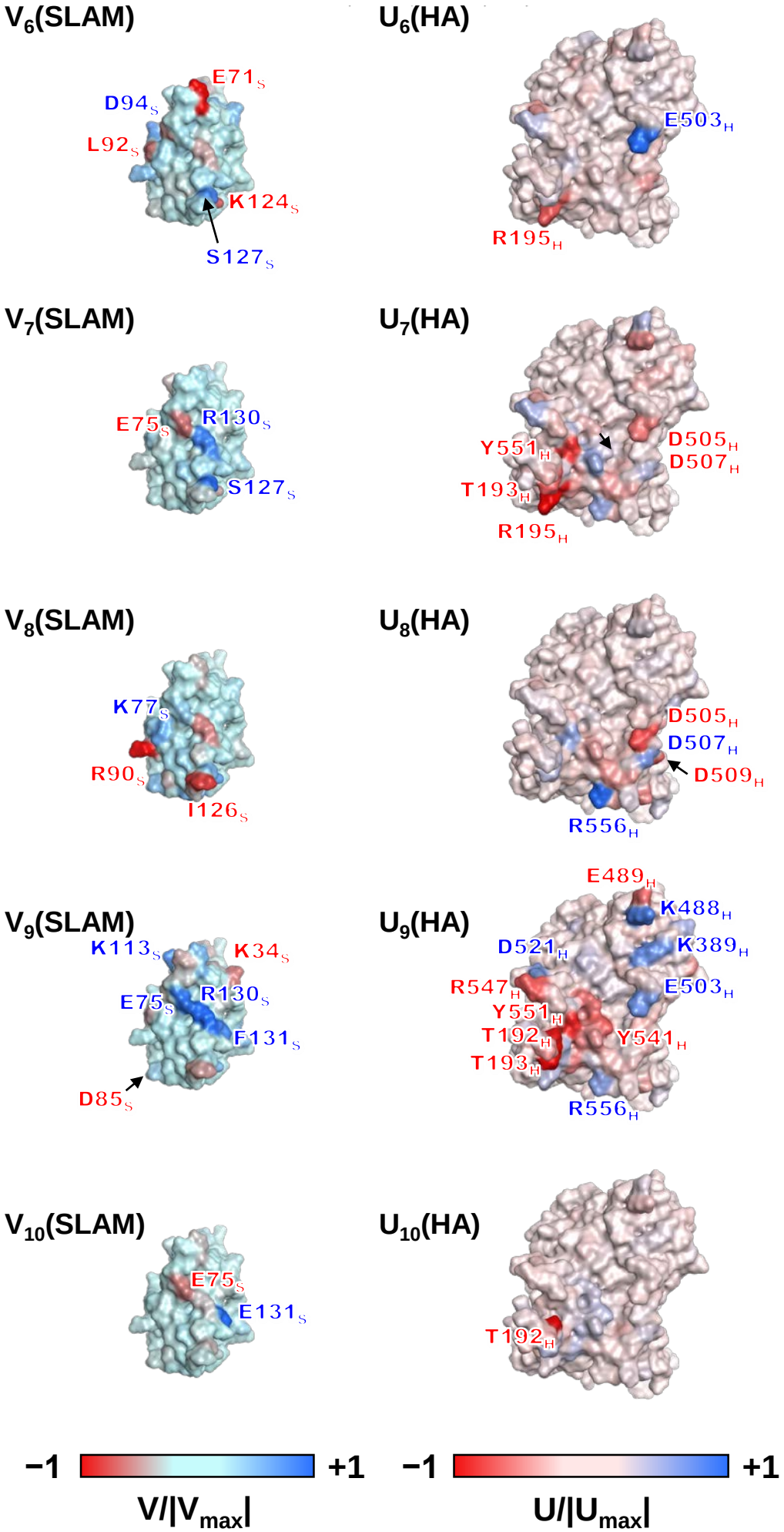

Figure. 4

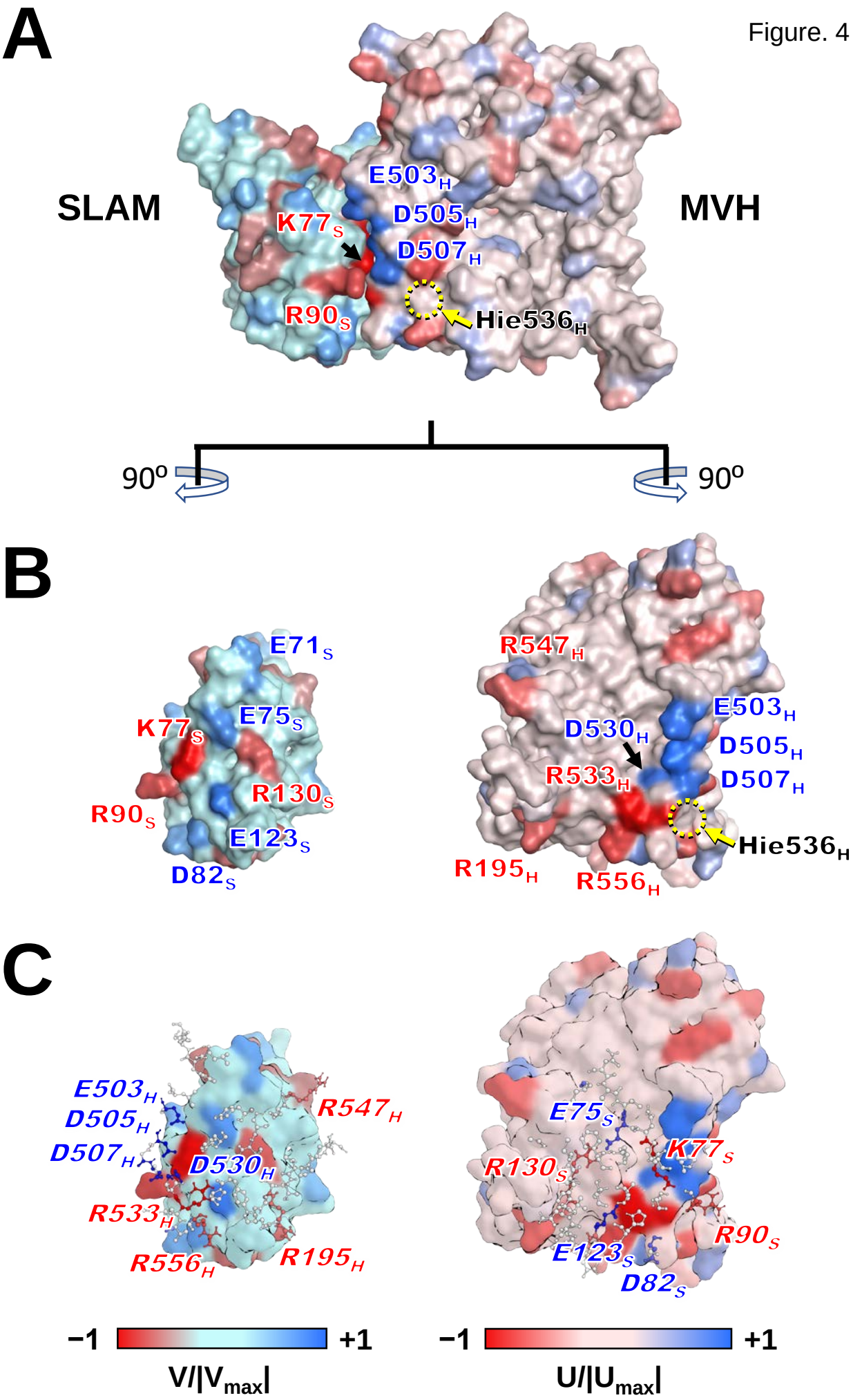
A
SLAM
MVH
E503H
D505H
D507H
K77S
R90S
Hie536H
90º
90º
B
E71S
E75S
K77S
R130S
R90S
E123S
D82S
R547H
E503H
D530H
D505H
R533H
D507H
Hie536H
R195H
R556H
C
E503H
D505H
D507H
R547H
D530H
R533H
R556H
R195H
E75S
K77S
R130S
R90S
E123S
D82S
−1
+1
V/|Vmax|
−1
+1
U/|Umax|

Figure. 5

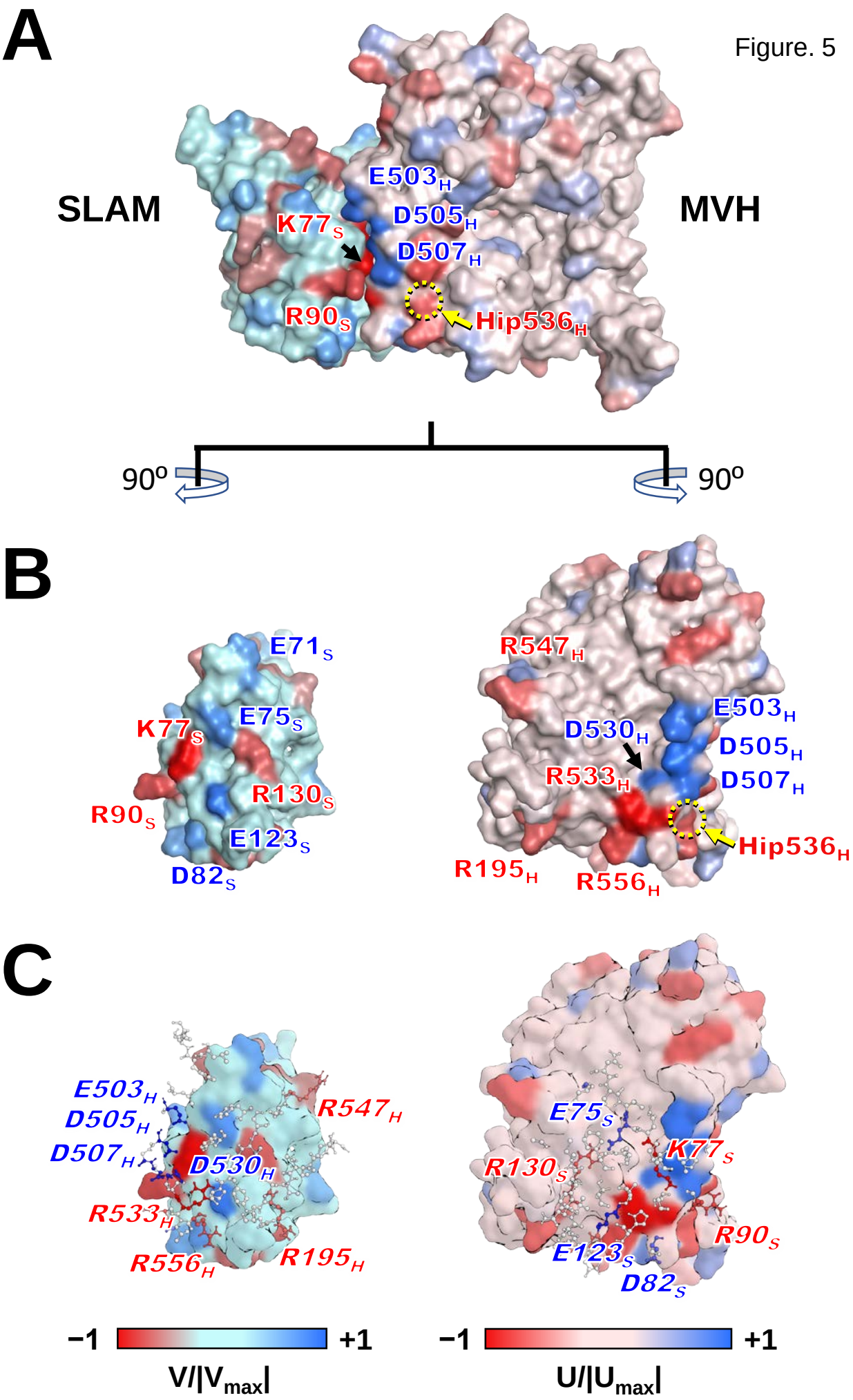
A
SLAM
MVH
E503H
D505H
D507H
K77S
R90S
Hip536H
90º
90º
B
E71S
E75S
K77S
R130S
R90S
E123S
D82S
R547H
E503H
D530H
D505H
R533H
D507H
Hip536H
R195H
R556H
C
E503H
D505H
D507H
R547H
D530H
R533H
R556H
R195H
E75S
K77S
R130S
R90S
E123S
D82S
−1
+1
V/|Vmax|
−1
+1
U/|Umax|

Figure. 6

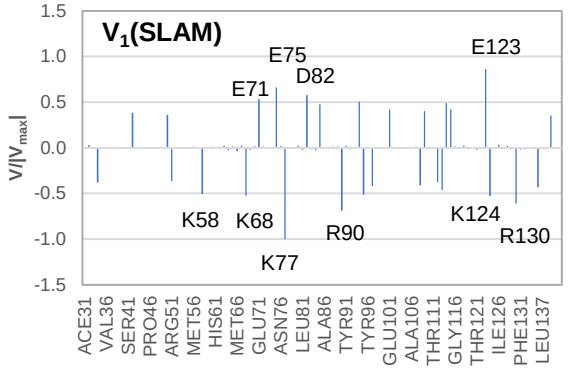
V1(SLAM)
V/|Vmax|
1.5
1.0
0.5
0.0
-0.5
-1.0
-1.5
E75
E123
D82
E71
K58
K68
K77
R90
K124
R130
ACE31
VAL36
SER41
PRO46
ARG51
MET56
HIS61
MET66
GLU71
ASN76
LEU81
ALA86
TYR91
TYR96
GLU101
ALA106
THR111
GLY116
THR121
ILE126
PHE131
LEU137

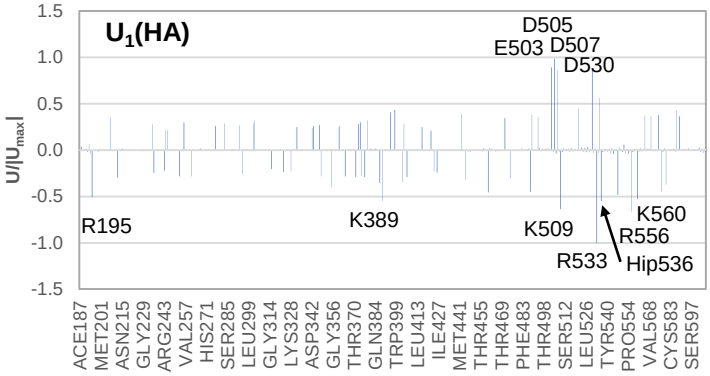
U1(HA)
U/|Umax|
1.5
1.0
0.5
0.0
-0.5
-1.0
-1.5
D505
E503
D507
D530
R195
K389
K509
K560
R556
R533
Hip536
ACE187
MET201
ASN215
GLY229
ARG243
VAL257
HIS271
SER285
LEU299
GLY314
LYS328
ASP342
GLY356
THR370
GLN384
TRP399
LEU413
ILE427
MET441
THR455
THR469
PHE483
THR498
SER512
LEU526
TYR540
PRO554
VAL568
CYS583
SER597

Figure. 7

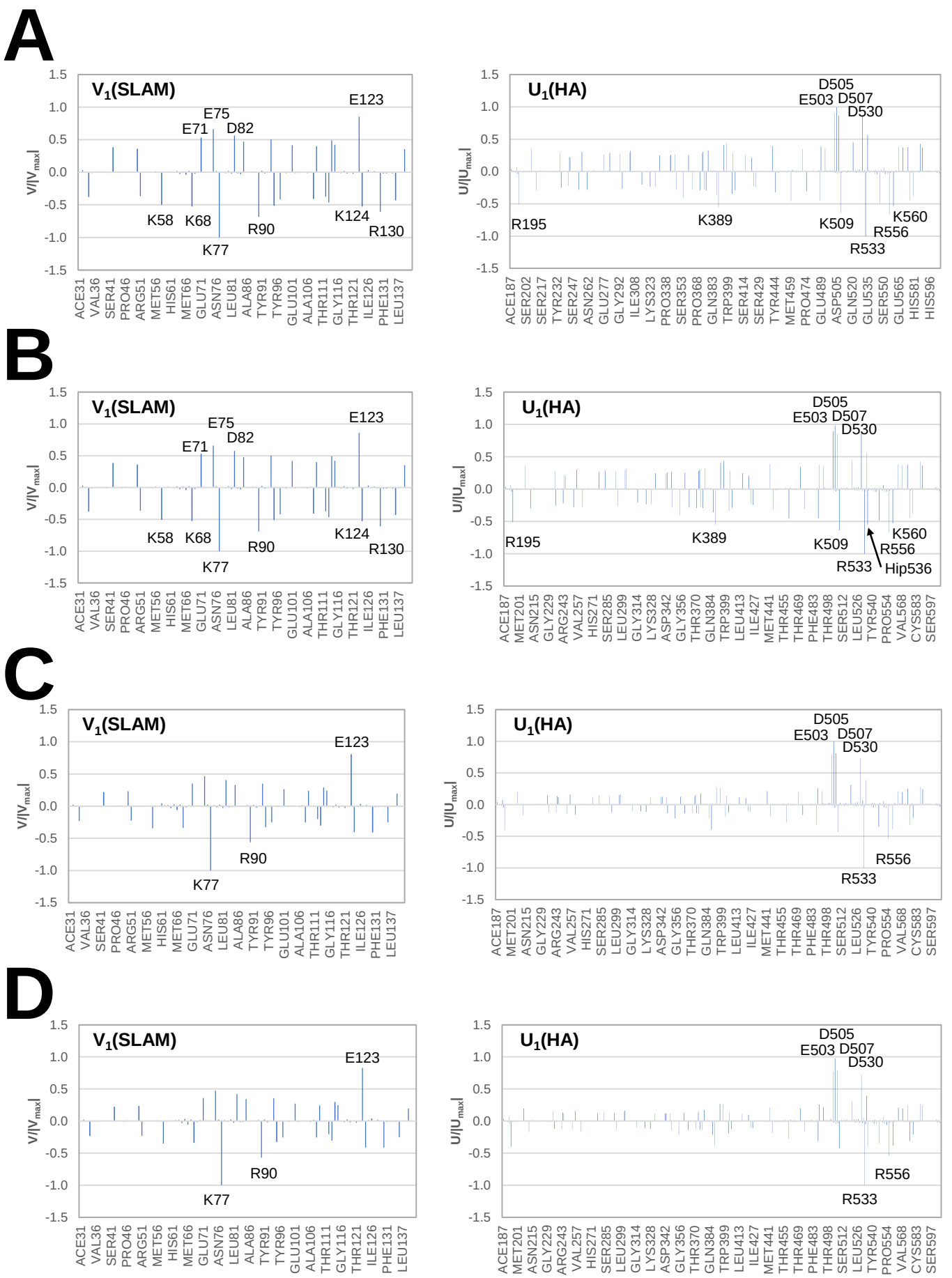
A
V1(SLAM)
E123
E75
E71
D82
K58
K68
K77
R90
K124
R130
U1(HA)
D505
E503 D507
D530
R195
K389
K509
K560
R556
R533
B
V1(SLAM)
E123
E75
E71
D82
K58
K68
K77
R90
K124
R130
U1(HA)
D505
E503 D507
D530
R195
K389
K509
K560
R556
R533
Hip536
C
V1(SLAM)
E123
R90
K77
U1(HA)
D505
E503
D507
D530
R556
R533
D
V1(SLAM)
E123
R90
K77
U1(HA)
D505
E503 D507
D530
R556
R533

Figure. 8

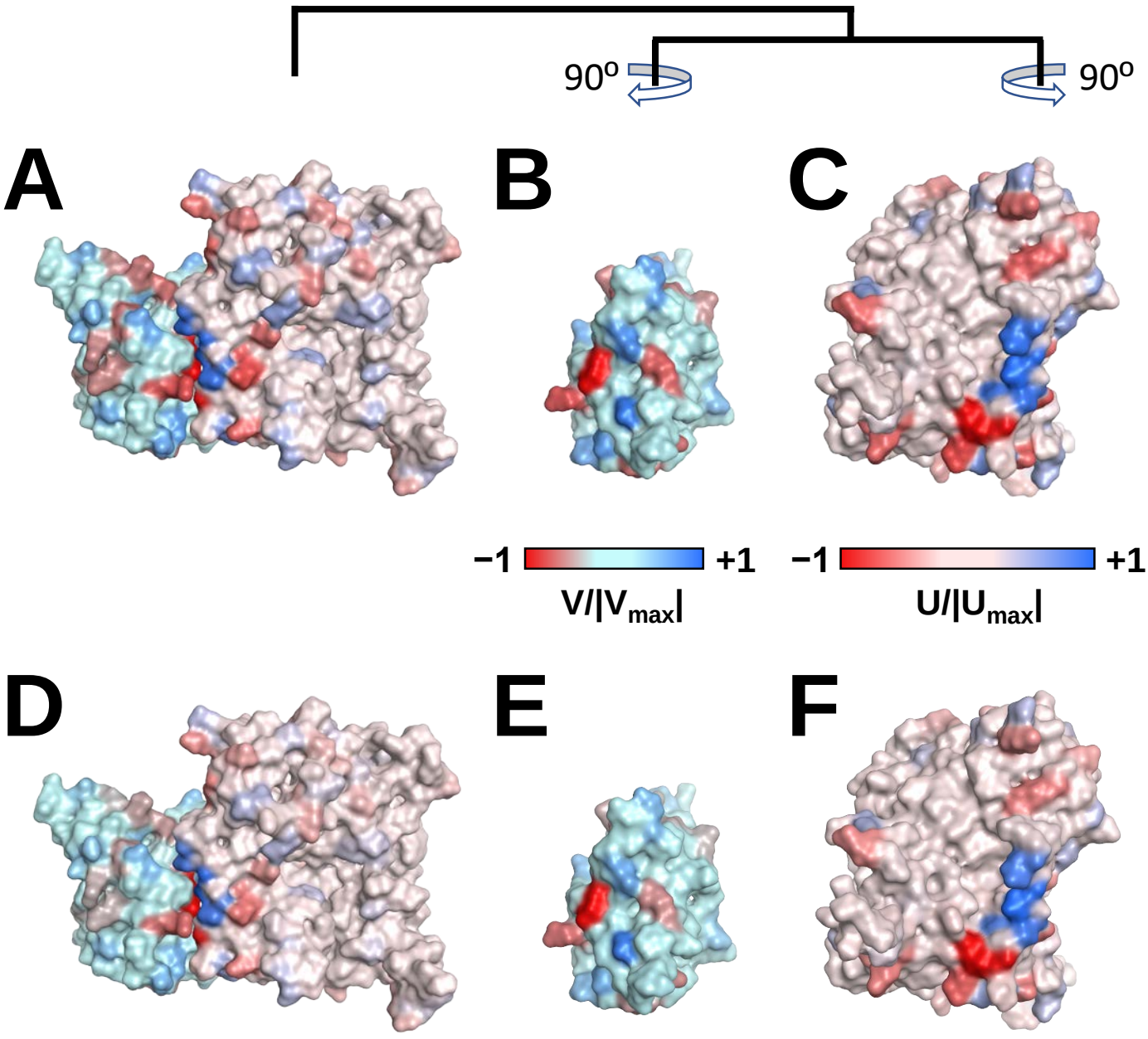

Table 1

Vector #	IFIE with Hie536			IFIE with Hip536		
	Singular value	Fraction	Accumulated occupancy	Singular value	Fraction	Accumulated occupancy
1	449.315	0.448	0.448	454.644	0.450	0.450
2	116.423	0.116	0.564	116.755	0.115	0.565
3	103.481	0.103	0.668	103.951	0.103	0.668
4	54.745	0.055	0.722	56.152	0.056	0.723
5	41.031	0.041	0.763	41.672	0.041	0.764
6	33.864	0.034	0.797	33.840	0.033	0.798
7	26.555	0.026	0.824	26.636	0.026	0.824
8	20.892	0.021	0.844	21.317	0.021	0.845
9	16.677	0.017	0.861	16.755	0.017	0.862
10	15.722	0.016	0.877	15.739	0.016	0.877
	SCIFIE with Hie536			**SCIFIE with Hip536**		
Vector #	**Singular value**	**Fraction**	**Accumulated occupancy**	**Singular value**	**Fraction**	**Accumulated occupancy**
1	230.852	0.308	0.308	233.106	0.308	0.308
2	102.076	0.136	0.444	103.161	0.137	0.445
3	93.085	0.124	0.568	92.962	0.123	0.568
4	49.857	0.066	0.634	50.687	0.067	0.635
5	37.755	0.050	0.685	38.480	0.051	0.686
6	32.755	0.044	0.728	32.722	0.043	0.729
7	25.730	0.034	0.763	25.701	0.034	0.763
8	20.975	0.028	0.791	20.996	0.028	0.791
9	17.845	0.024	0.814	17.969	0.024	0.815
10	15.743	0.021	0.835	15.757	0.021	0.836

Supplementary data for "Identification of correlated inter-residue interactions in protein complex based on the fragment molecular orbital method"

Shigenori Tanaka

Graduate School of System Informatics, Department of Computational Science, Kobe University, 1-1 Rokkodai, Nada-ku, Kobe 657-8501, Japan

Chiduru Watanabe

Center for Biosystems Dynamics Research, RIKEN, 1-7-22 Suehiro-cho, Tsurumi-ku, Yokohama, Kanagawa 230-0045, Japan
& JST PRESTO, 4-1-8, Honcho, Kawaguchi, Saitama 332-0012 Japan

Teruki Honma

Center for Biosystems Dynamics Research, RIKEN, 1-7-22 Suehiro-cho, Tsurumi-ku, Yokohama, Kanagawa 230-0045, Japan

Kaori Fukuzawa

Department of Physical Chemistry, School of Pharmacy and Pharmaceutical Sciences, Hoshi University, 2-4-41 Ebara, Shinagawa, Tokyo 142-8501, Japan

Kazue Ohishi

Faculty of Engineering, Tokyo Polytechnic University, 1583, Iiyama, Atsugi, Kanagawa 243-0297, Japan

Tadashi Maruyama

Kitasato University, 1-15-1, Kitazato, Minami, Sagamihara, Kanagawa 252-0373, Japan

Email address: tanaka2@kobe-u.ac.jp; Fax:+81-78-803-6621 (Shigenori Tanaka)

Supplementary figures

In this document, supplementary figures S1-S4 for the singular eigenvectors are given with their legends.

Figure captions

Figure S1: Singular vectors 1-10 with decreasing singular values for SLAM (left, V_1-V_{10}) and HA (right, U_1-U_{10}), where the IFIE values were obtained by the FMO calculation in which Hip536 was employed. The abscissa refers to the amino-acid numbers and the ordinate represents the values of singular vector components normalized by the maximum value.

Figure S2: Residues with large magnitude in each singular vector 1-10 for SLAM (left, V_1-V_{10}) and HA (right, U_1-U_{10}). The IFIE values used for the SVD analysis were the same as those in Fig. S1. Blue and red colors indicate positive and negative values, respectively, whose deepness of the hue refers to the normalized magnitude.

Figure S3: Singular vectors 1-10 with decreasing singular values for SLAM (left, V_1-V_{10}) and HA (right, U_1-U_{10}) in the case that the SCIFIE values were used. The SCIFIE values for the SVD were obtained through the FMO calculation in which Hie536 was employed. The abscissa refers to the amino-acid numbers and the ordinate represents the values of singular vector components normalized by the maximum value.

Figure S4: Singular vectors 1-10 with decreasing singular values for SLAM (left, V_1-V_{10}) and HA (right, U_1-U_{10}) in the case that the SCIFIE values obtained through the FMO calculation with Hip536 were employed. The abscissa refers to the amino-acid numbers and the ordinate represents the values of singular vector components normalized by the maximum value.

Figure. S1

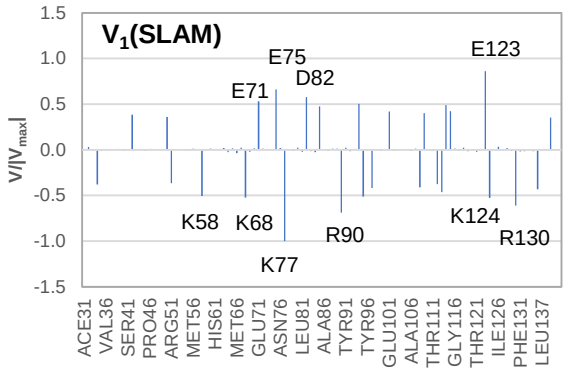
V1(SLAM)
E75
E123
E71
D82
K58
K68
K124
R90
R130
K77
|V/|Vmax|
ACE31 VAL36 SER41 PRO46 ARG51 MET56 HIS61 MET66 GLU71 ASN76 LEU81 ALA86 TYR91 TYR96 GLU101 ALA106 THR111 GLY116 THR121 ILE126 PHE131 LEU137

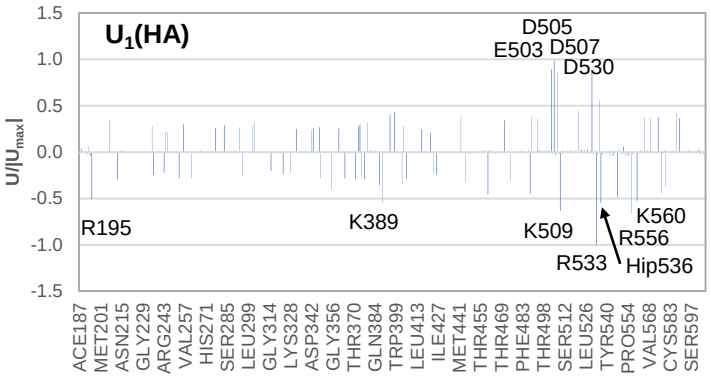
U1(HA)
D505
E503 D507
D530
R195
K389
K509
K560
R556
R533
Hip536
|U/|Umax|
ACE187 MET201 ASN215 GLY229 ARG243 VAL257 HIS271 SER285 LEU299 GLY314 LYS328 ASP342 GLY356 THR370 GLN384 TRP399 LEU413 ILE427 MET441 THR455 THR469 PHE483 THR498 SER512 LEU526 TYR540 PRO554 VAL568 CYS583 SER597

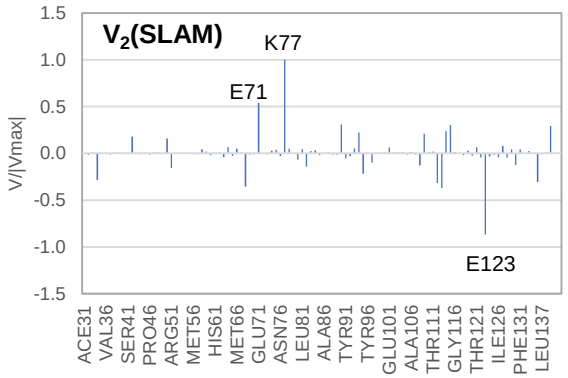
V2(SLAM)
K77
E71
E123
V/|Vmax|
ACE31 VAL36 SER41 PRO46 ARG51 MET56 HIS61 MET66 GLU71 ASN76 LEU81 ALA86 TYR91 TYR96 GLU101 ALA106 THR111 GLY116 THR121 ILE126 PHE131 LEU137

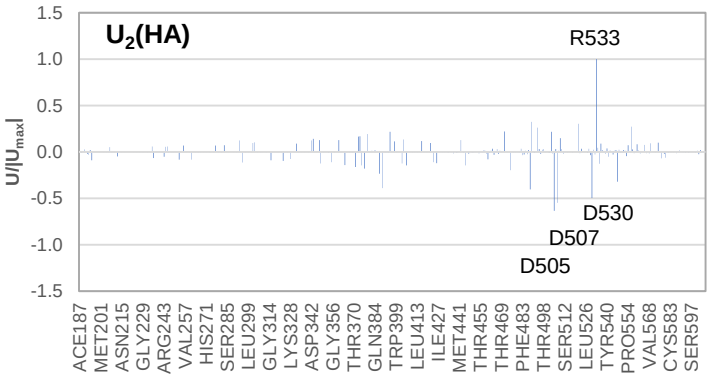
U2(HA)
R533
D530
D507
D505
|U/|Umax|
ACE187 MET201 ASN215 GLY229 ARG243 VAL257 HIS271 SER285 LEU299 GLY314 LYS328 ASP342 GLY356 THR370 GLN384 TRP399 LEU413 ILE427 MET441 THR455 THR469 PHE483 THR498 SER512 LEU526 TYR540 PRO554 VAL568 CYS583 SER597

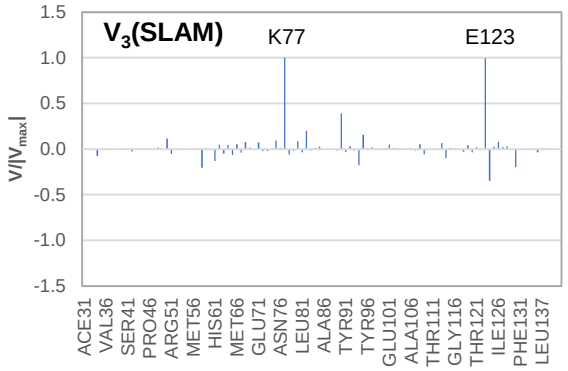
V3(SLAM)
K77
E123
|V/|Vmax|
ACE31 VAL36 SER41 PRO46 ARG51 MET56 HIS61 MET66 GLU71 ASN76 LEU81 ALA86 TYR91 TYR96 GLU101 ALA106 THR111 GLY116 THR121 ILE126 PHE131 LEU137

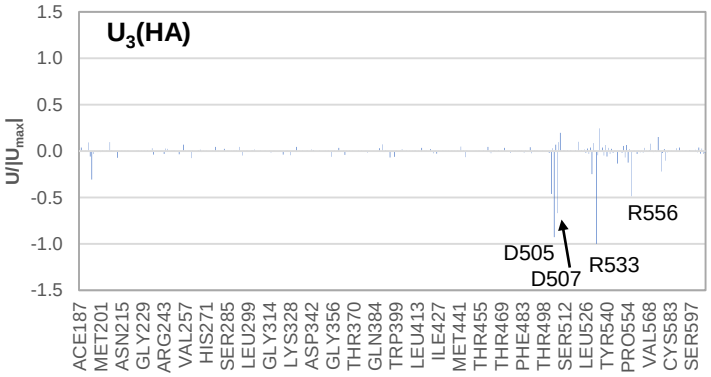
U3(HA)
R556
D505
D507
R533
|U/|Umax|
ACE187 MET201 ASN215 GLY229 ARG243 VAL257 HIS271 SER285 LEU299 GLY314 LYS328 ASP342 GLY356 THR370 GLN384 TRP399 LEU413 ILE427 MET441 THR455 THR469 PHE483 THR498 SER512 LEU526 TYR540 PRO554 VAL568 CYS583 SER597

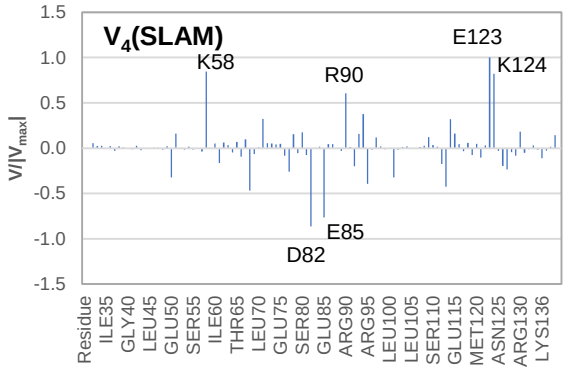
V4(SLAM)
E123
K58
K124
R90
E85
D82
|V/|Vmax|
Residue ILE35 GLY40 LEU45 GLU50 SER55 ILE60 THR65 LEU70 GLU75 SER80 GLU85 ARG90 ARG95 LEU100 LEU105 SER110 GLU115 MET120 ASN125 ARG130 LYS136

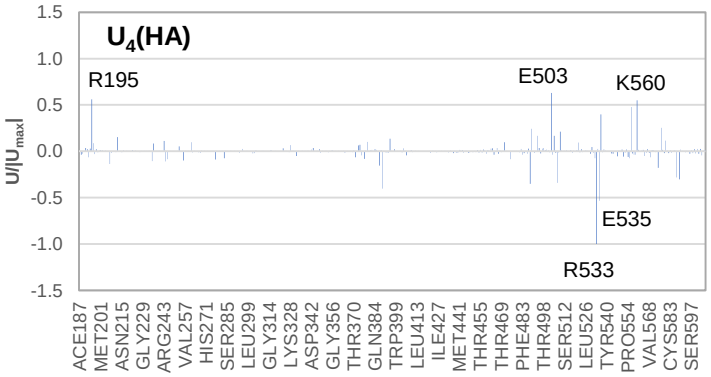
U4(HA)
R195
E503
K560
E535
R533
|U/|Umax|
ACE187 MET201 ASN215 GLY229 ARG243 VAL257 HIS271 SER285 LEU299 GLY314 LYS328 ASP342 GLY356 THR370 GLN384 TRP399 LEU413 ILE427 MET441 THR455 THR469 PHE483 THR498 SER512 LEU526 TYR540 PRO554 VAL568 CYS583 SER597

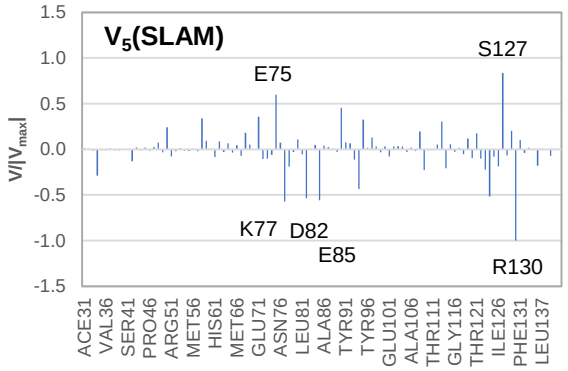
V5(SLAM)
S127
E75
K77
D82
E85
R130
|V/|Vmax|
ACE31 VAL36 SER41 PRO46 ARG51 MET56 HIS61 MET66 GLU71 ASN76 LEU81 ALA86 TYR91 TYR96 GLU101 ALA106 THR111 GLY116 THR121 ILE126 PHE131 LEU137

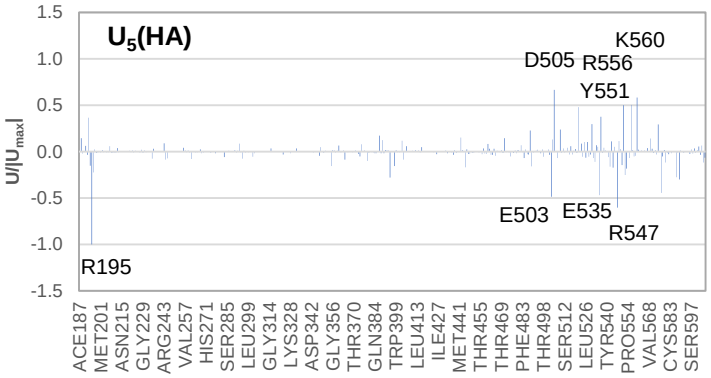
U5(HA)
K560
D505 R556
Y551
E503
E535
R547
R195
|U/|Umax|
ACE187 MET201 ASN215 GLY229 ARG243 VAL257 HIS271 SER285 LEU299 GLY314 LYS328 ASP342 GLY356 THR370 GLN384 TRP399 LEU413 ILE427 MET441 THR455 THR469 PHE483 THR498 SER512 LEU526 TYR540 PRO554 VAL568 CYS583 SER597

Figure. S1 (continued)

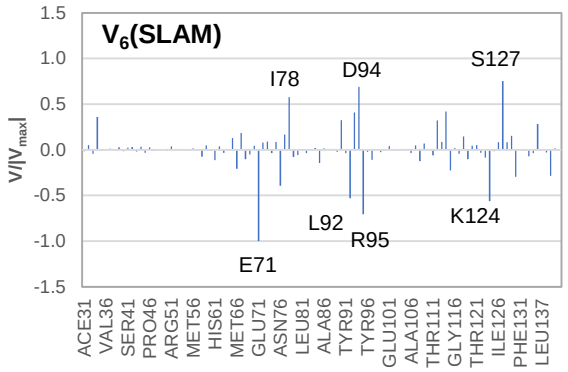

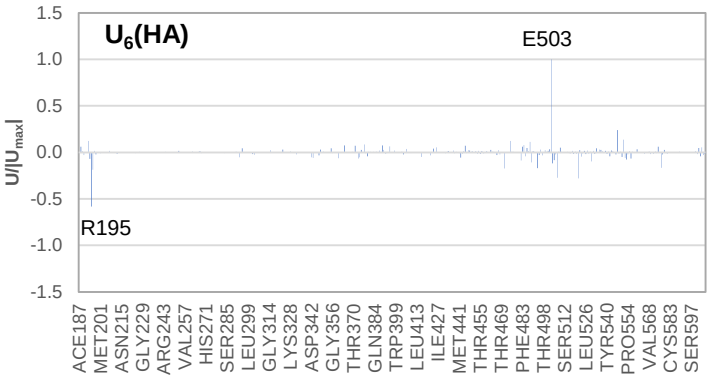

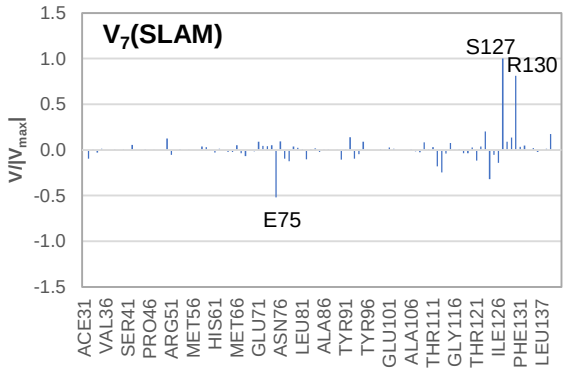

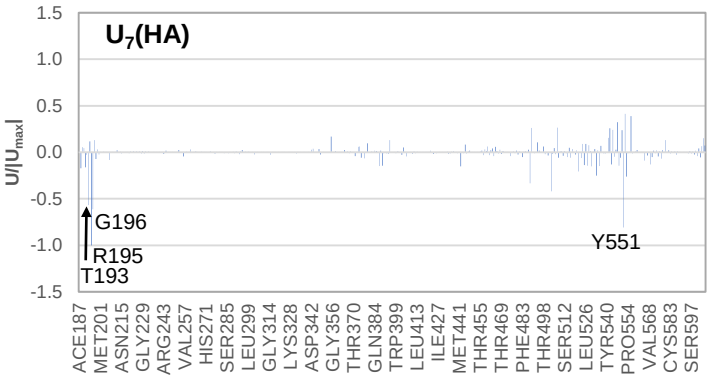

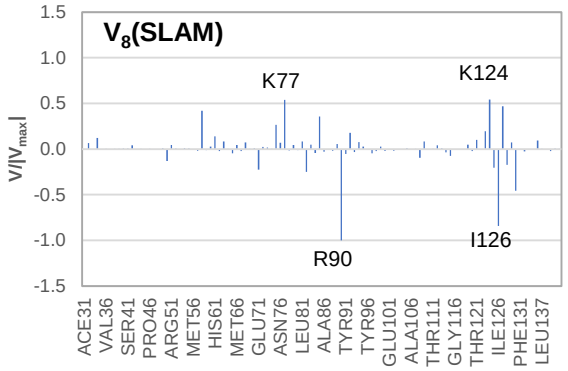

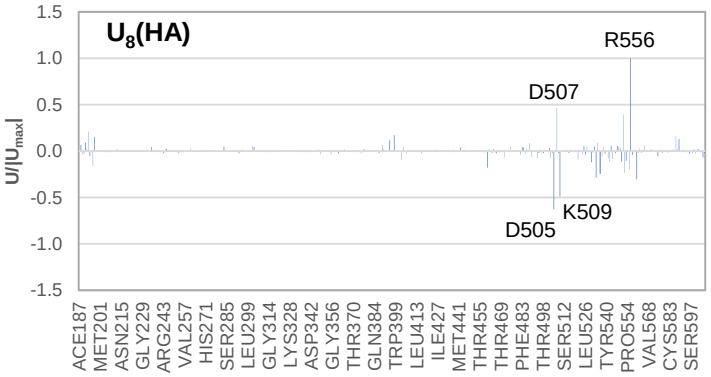

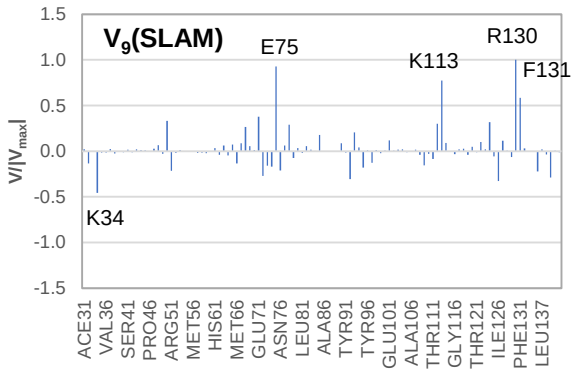

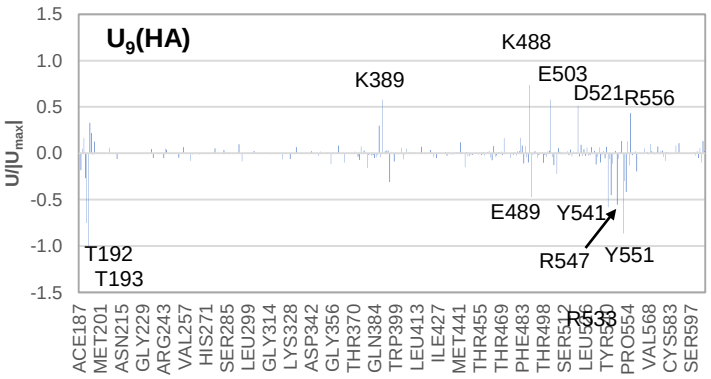

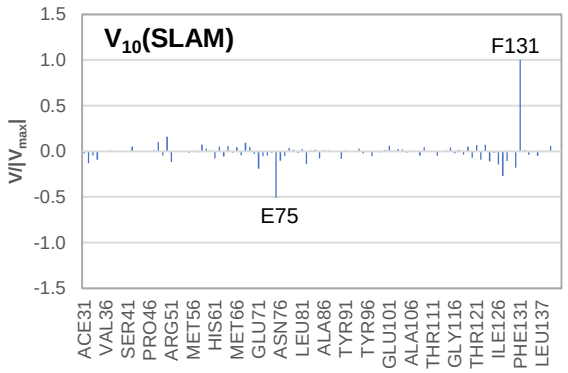

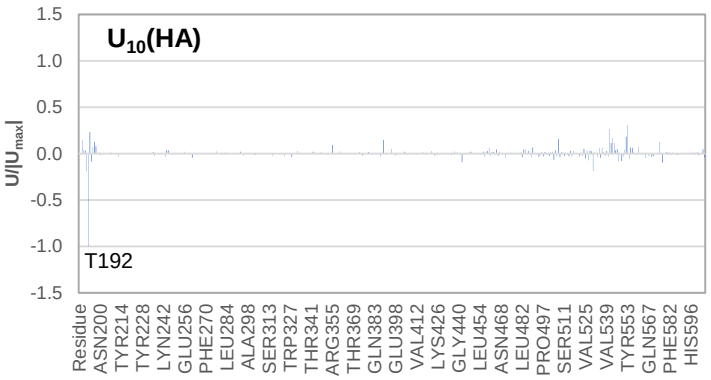

Figure. S2

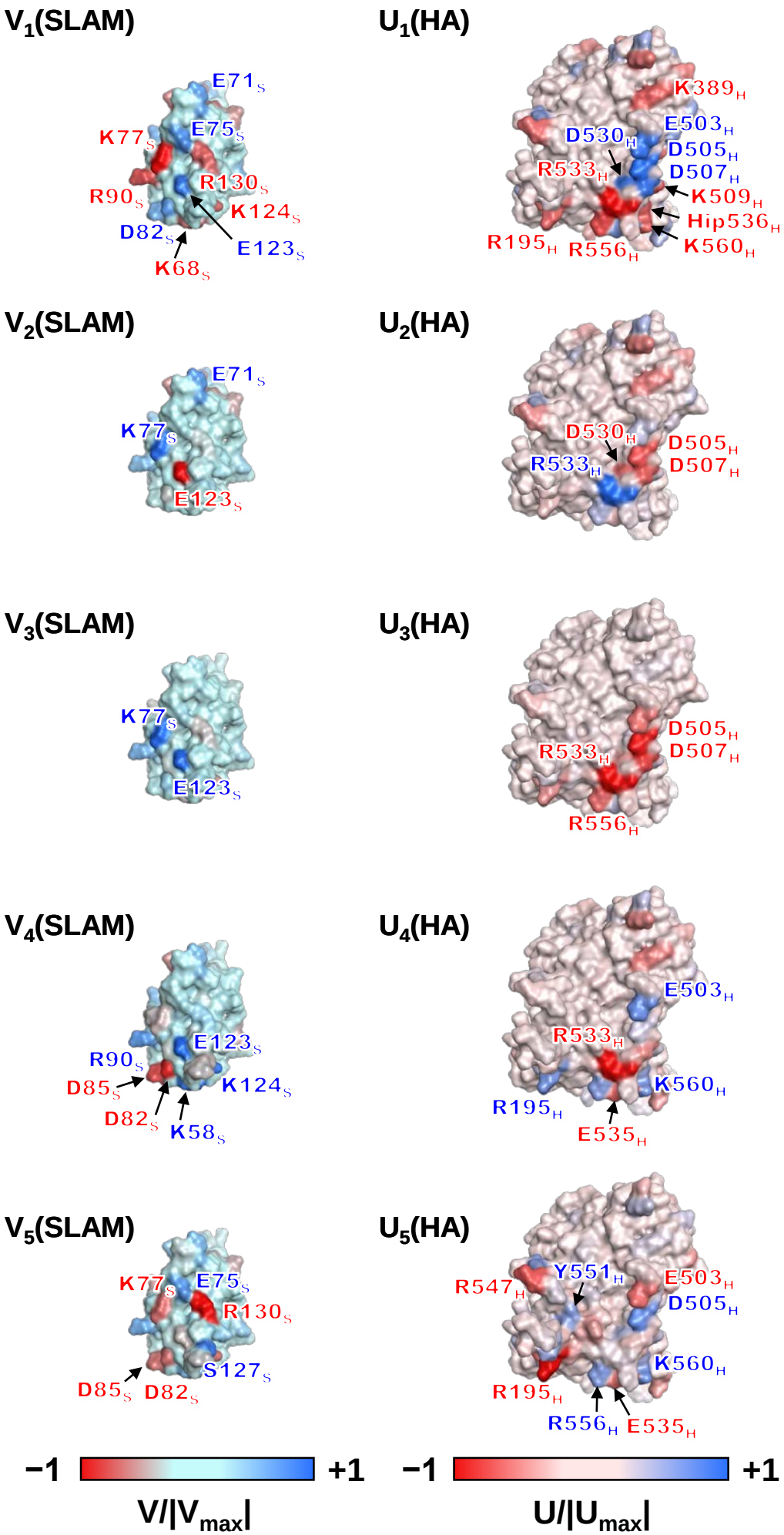
V1(SLAM)
E71S
K77S
E75S
R130S
R90S
K124S
D82S
E123S
K68S
U1(HA)
K389H
E503H
D530H
D505H
R533H
D507H
K509H
Hip536H
R195H
R556H
K560H
V2(SLAM)
E71S
K77S
E123S
U2(HA)
D530H
D505H
R533H
D507H
V3(SLAM)
K77S
E123S
U3(HA)
D505H
R533H
D507H
R556H
V4(SLAM)
E123S
R90S
D85S
K124S
D82S
K58S
U4(HA)
E503H
R533H
K560H
R195H
E535H
V5(SLAM)
K77S
E75S
R130S
S127S
D85S
D82S
U5(HA)
R547H
Y551H
E503H
D505H
K560H
R195H
R556H
E535H
−1
+1
V/|Vmax|
−1
+1
U/|Umax|

Figure. S2 (continued)

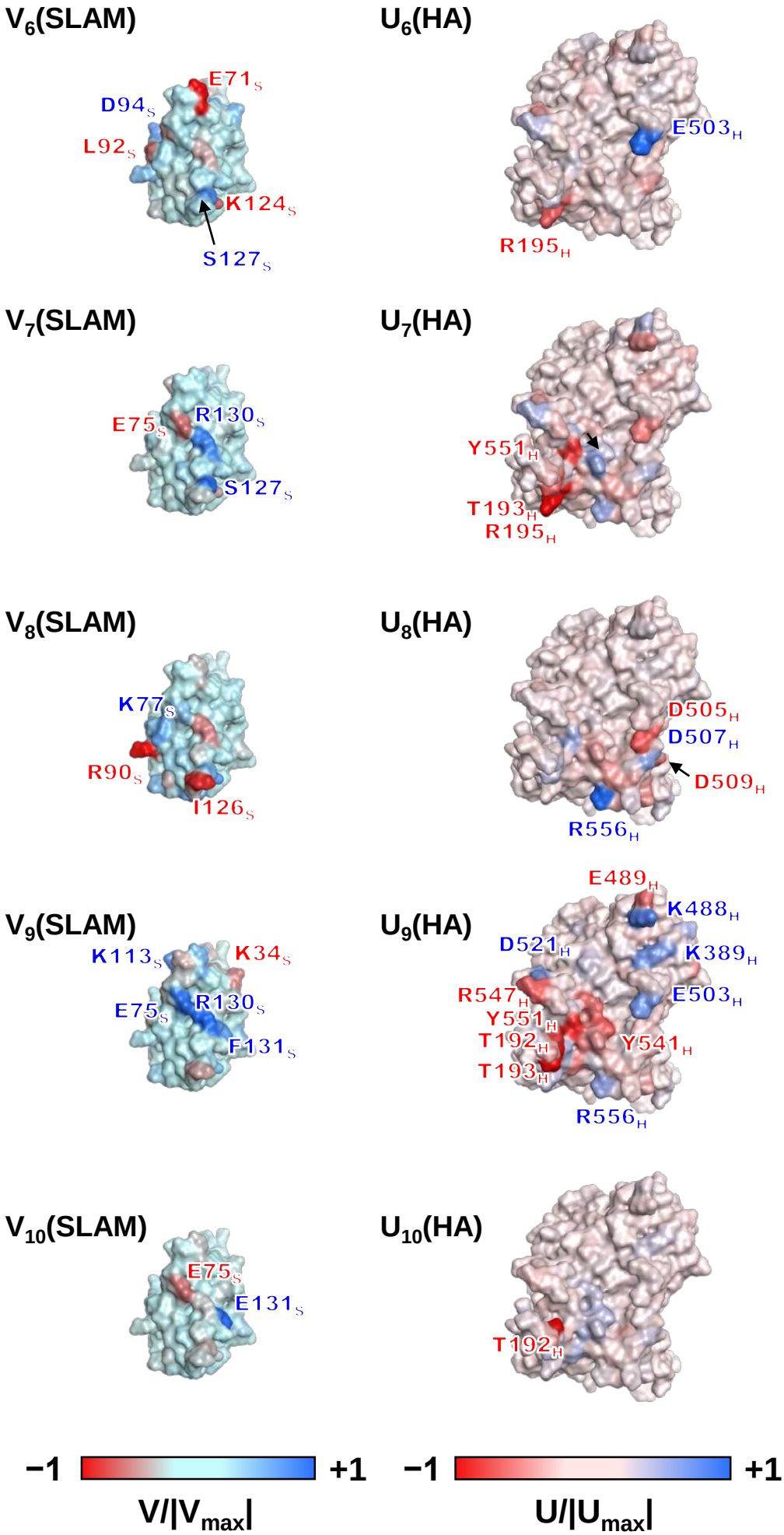

Figure. S3

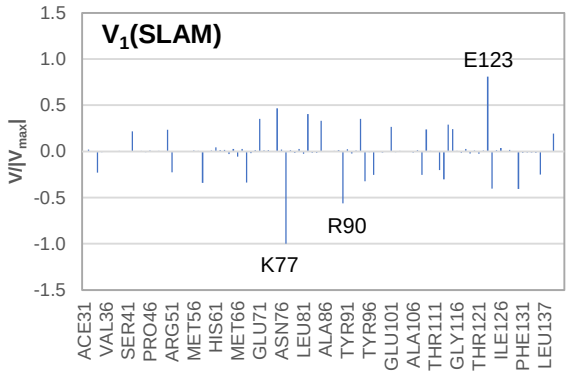
V1(SLAM)
E123
R90
K77
V/|Vmax|
ACE31 VAL36 SER41 PRO46 ARG51 MET56 HIS61 MET66 GLU71 ASN76 LEU81 ALA86 TYR91 TYR96 GLU101 ALA106 THR111 GLY116 THR121 ILE126 PHE131 LEU137

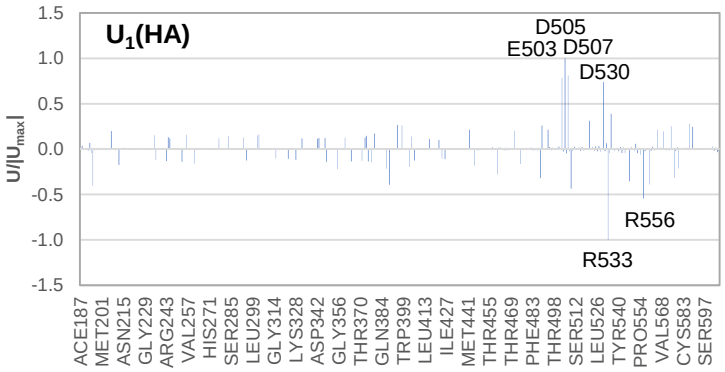
U1(HA)
D505
E503 D507
D530
R556
R533
U/|Umax|
ACE187 MET201 ASN215 GLY229 ARG243 VAL257 HIS271 SER285 LEU299 GLY314 LYS328 ASP342 GLY356 THR370 GLN384 TRP399 LEU413 ILE427 MET441 THR455 THR469 PHE483 THR498 SER512 LEU526 TYR540 PRO554 VAL568 CYS583 SER597

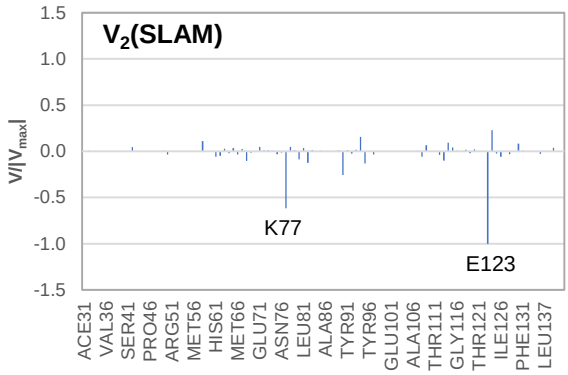
V2(SLAM)
K77
E123
V/|Vmax|
ACE31 VAL36 SER41 PRO46 ARG51 MET56 HIS61 MET66 GLU71 ASN76 LEU81 ALA86 TYR91 TYR96 GLU101 ALA106 THR111 GLY116 THR121 ILE126 PHE131 LEU137

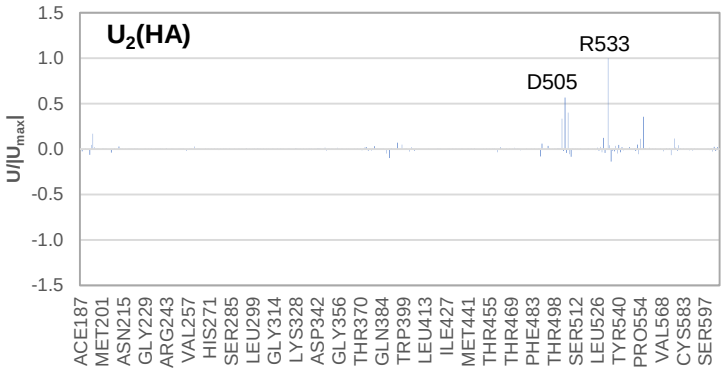
U2(HA)
R533
D505
U/|Umax|
ACE187 MET201 ASN215 GLY229 ARG243 VAL257 HIS271 SER285 LEU299 GLY314 LYS328 ASP342 GLY356 THR370 GLN384 TRP399 LEU413 ILE427 MET441 THR455 THR469 PHE483 THR498 SER512 LEU526 TYR540 PRO554 VAL568 CYS583 SER597

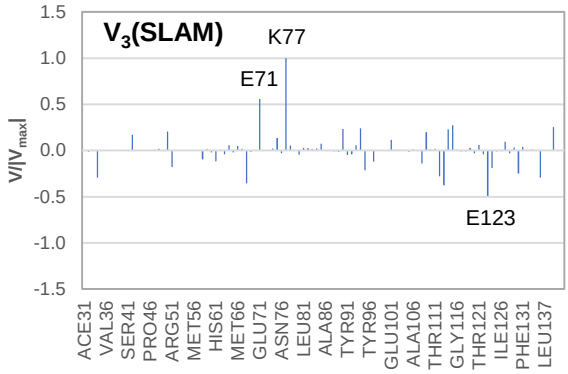
V3(SLAM)
K77
E71
E123
V/|Vmax|
ACE31 VAL36 SER41 PRO46 ARG51 MET56 HIS61 MET66 GLU71 ASN76 LEU81 ALA86 TYR91 TYR96 GLU101 ALA106 THR111 GLY116 THR121 ILE126 PHE131 LEU137

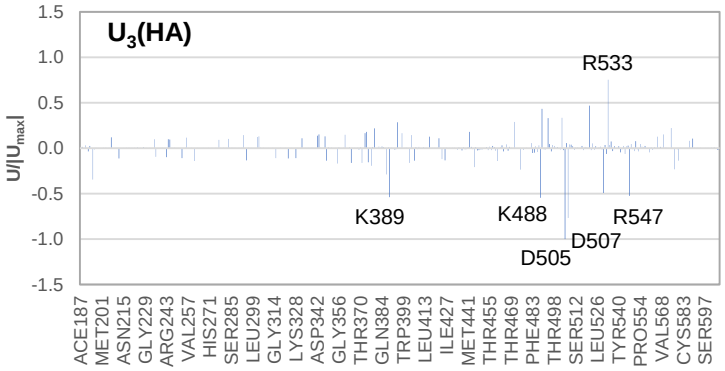
U3(HA)
R533
K389
K488
R547
D507
D505
U/|Umax|
ACE187 MET201 ASN215 GLY229 ARG243 VAL257 HIS271 SER285 LEU299 GLY314 LYS328 ASP342 GLY356 THR370 GLN384 TRP399 LEU413 ILE427 MET441 THR455 THR469 PHE483 THR498 SER512 LEU526 TYR540 PRO554 VAL568 CYS583 SER597

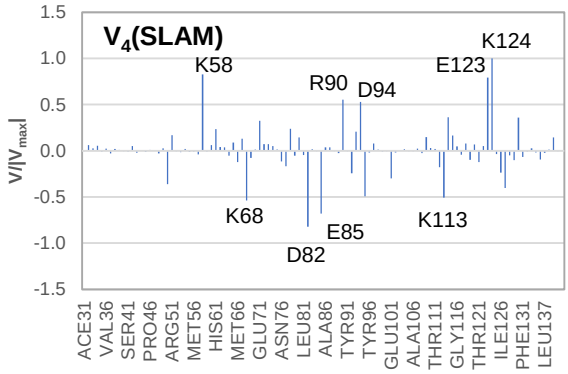
V4(SLAM)
K124
K58
E123
R90
D94
K68
E85
K113
D82
V/|Vmax|
ACE31 VAL36 SER41 PRO46 ARG51 MET56 HIS61 MET66 GLU71 ASN76 LEU81 ALA86 TYR91 TYR96 GLU101 ALA106 THR111 GLY116 THR121 ILE126 PHE131 LEU137

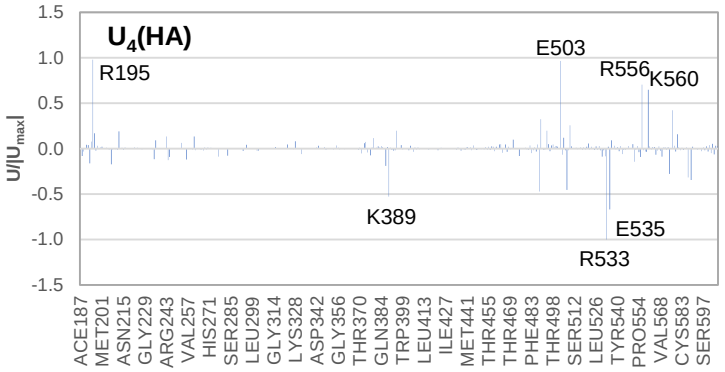
U4(HA)
E503
R195
R556
K560
K389
E535
R533
U/|Umax|
ACE187 MET201 ASN215 GLY229 ARG243 VAL257 HIS271 SER285 LEU299 GLY314 LYS328 ASP342 GLY356 THR370 GLN384 TRP399 LEU413 ILE427 MET441 THR455 THR469 PHE483 THR498 SER512 LEU526 TYR540 PRO554 VAL568 CYS583 SER597

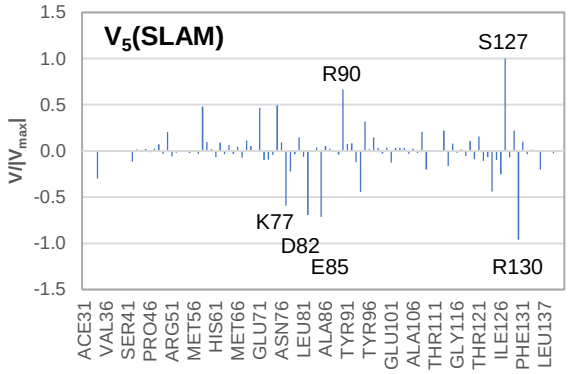
V5(SLAM)
S127
R90
K77
D82
E85
R130
V/|Vmax|
ACE31 VAL36 SER41 PRO46 ARG51 MET56 HIS61 MET66 GLU71 ASN76 LEU81 ALA86 TYR91 TYR96 GLU101 ALA106 THR111 GLY116 THR121 ILE126 PHE131 LEU137

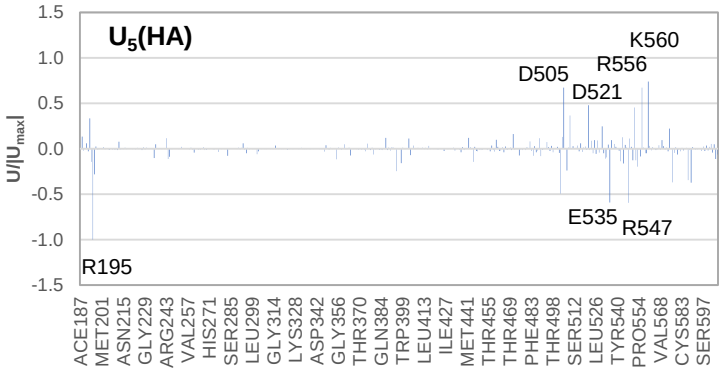
U5(HA)
K560
D505
R556
D521
E535
R547
R195
U/|Umax|
ACE187 MET201 ASN215 GLY229 ARG243 VAL257 HIS271 SER285 LEU299 GLY314 LYS328 ASP342 GLY356 THR370 GLN384 TRP399 LEU413 ILE427 MET441 THR455 THR469 PHE483 THR498 SER512 LEU526 TYR540 PRO554 VAL568 CYS583 SER597

Figure. S3 (continued)

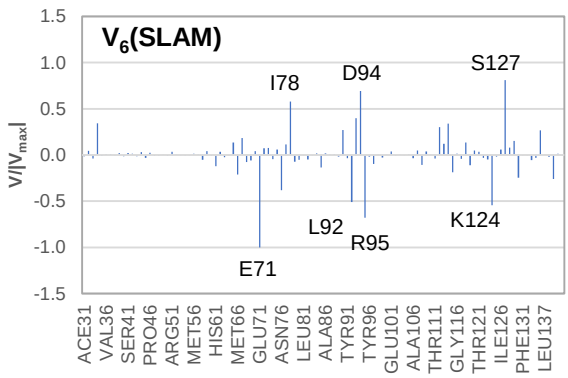

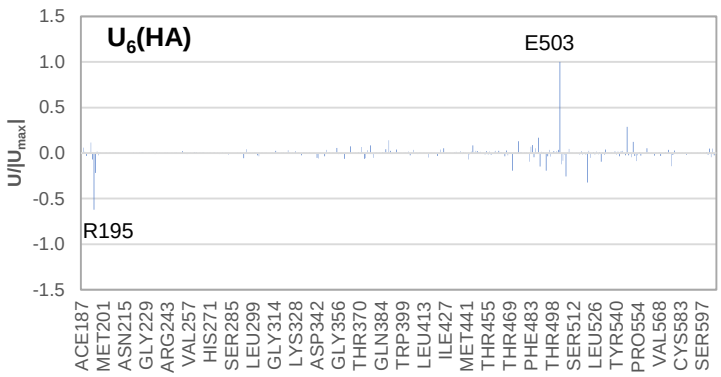

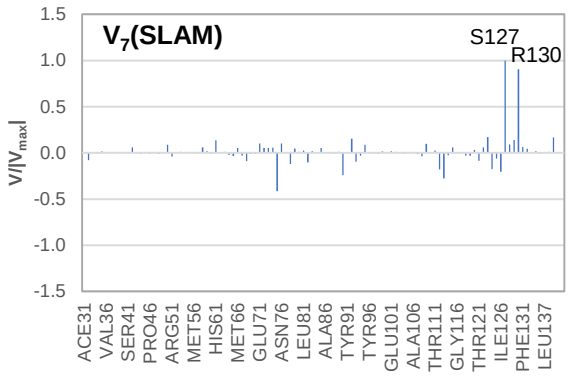

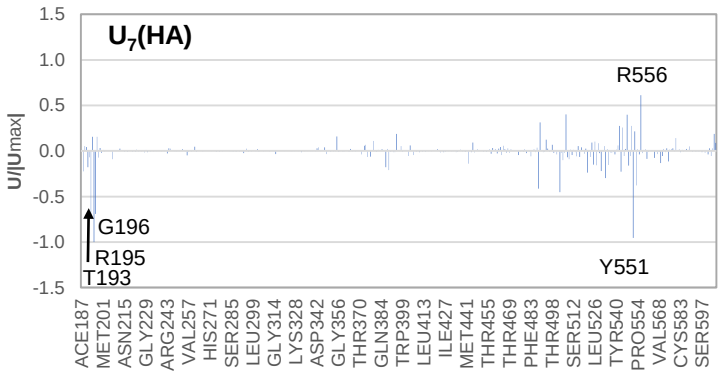

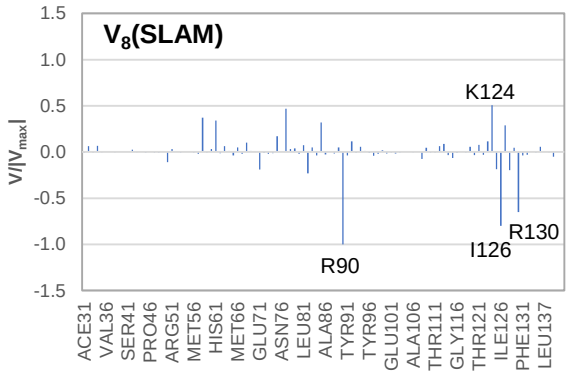

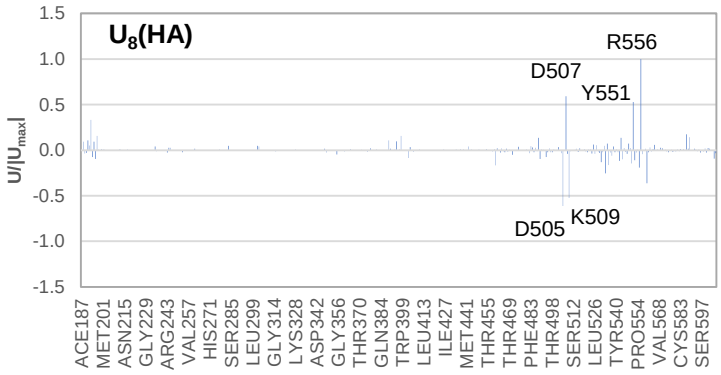

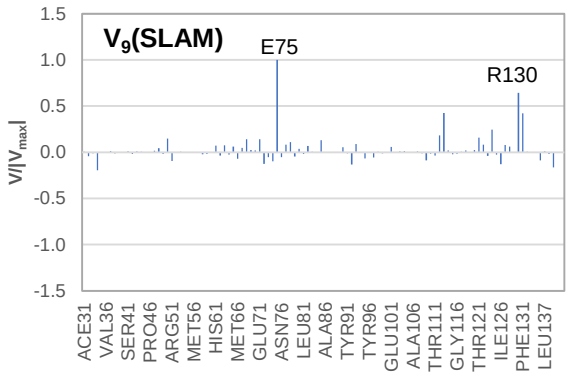

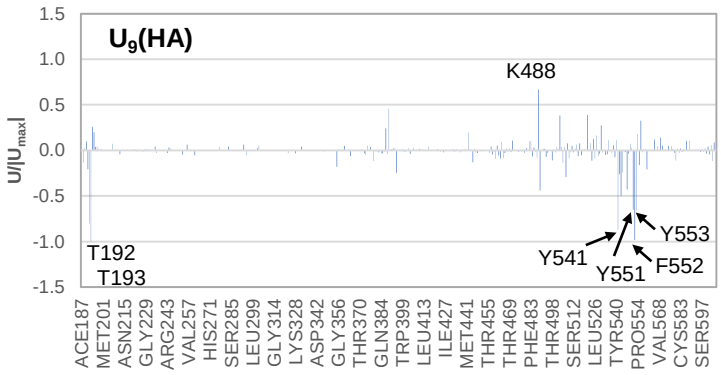

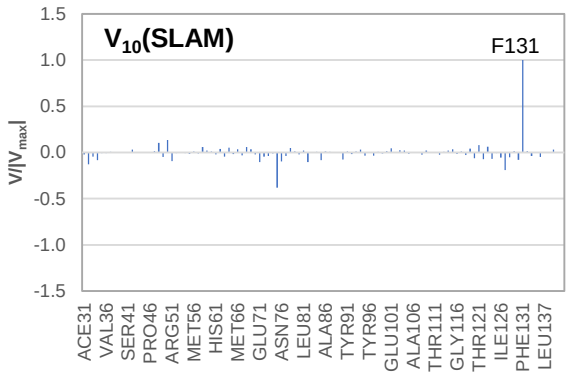

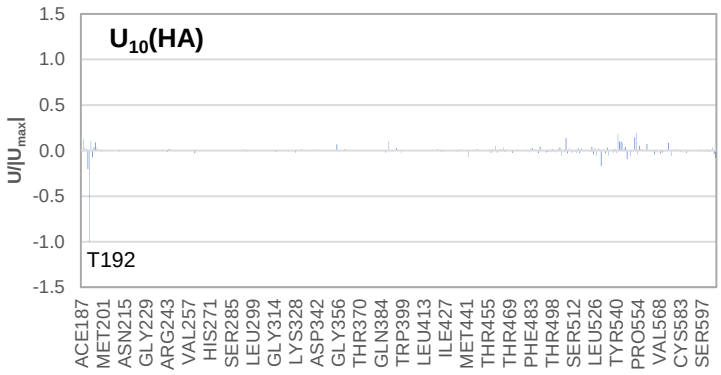

Figure. S4

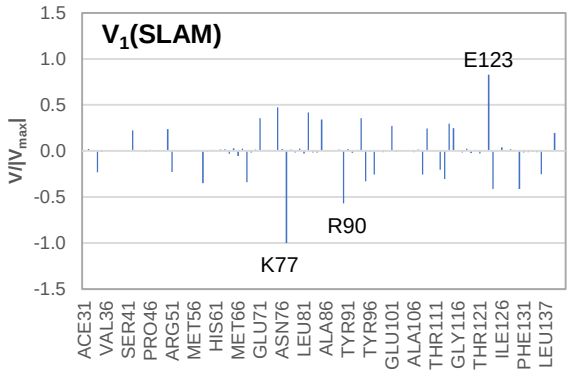
V1(SLAM)
E123
R90
K77
V/|Vmax|
ACE31 VAL36 SER41 PRO46 ARG51 MET56 HIS61 MET66 GLU71 ASN76 LEU81 ALA86 TYR91 TYR96 GLU101 ALA106 THR111 GLY116 THR121 ILE126 PHE131 LEU137

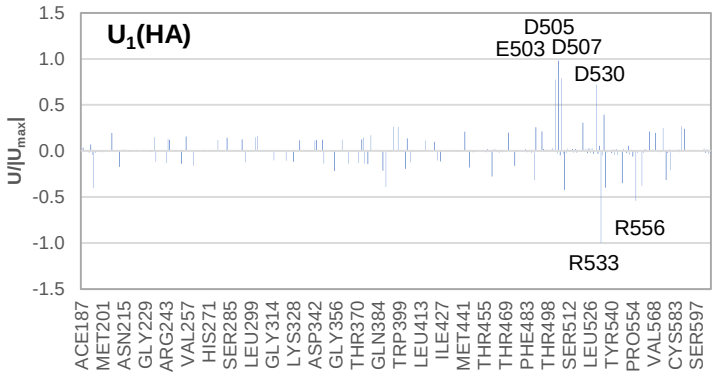
U1(HA)
D505
E503 D507
D530
R556
R533
U/|Umax|
ACE187 MET201 ASN215 GLY229 ARG243 VAL257 HIS271 SER285 LEU299 GLY314 LYS328 ASP342 GLY356 THR370 GLN384 TRP399 LEU413 ILE427 MET441 THR455 THR469 PHE483 THR498 SER512 LEU526 TYR540 PRO554 VAL568 CYS583 SER597

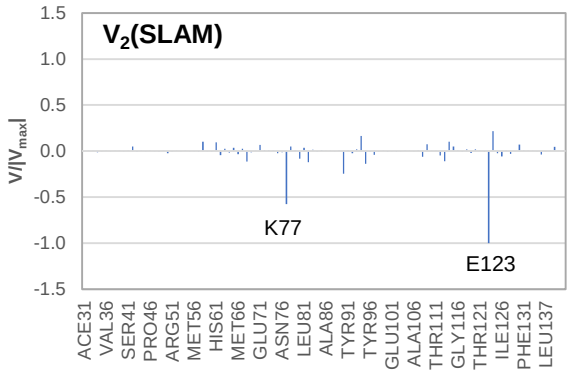
V2(SLAM)
K77
E123
V/|Vmax|
ACE31 VAL36 SER41 PRO46 ARG51 MET56 HIS61 MET66 GLU71 ASN76 LEU81 ALA86 TYR91 TYR96 GLU101 ALA106 THR111 GLY116 THR121 ILE126 PHE131 LEU137

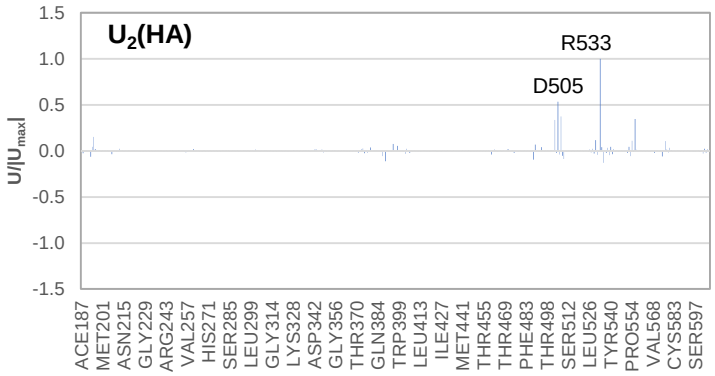
U2(HA)
R533
D505
U/|Umax|
ACE187 MET201 ASN215 GLY229 ARG243 VAL257 HIS271 SER285 LEU299 GLY314 LYS328 ASP342 GLY356 THR370 GLN384 TRP399 LEU413 ILE427 MET441 THR455 THR469 PHE483 THR498 SER512 LEU526 TYR540 PRO554 VAL568 CYS583 SER597

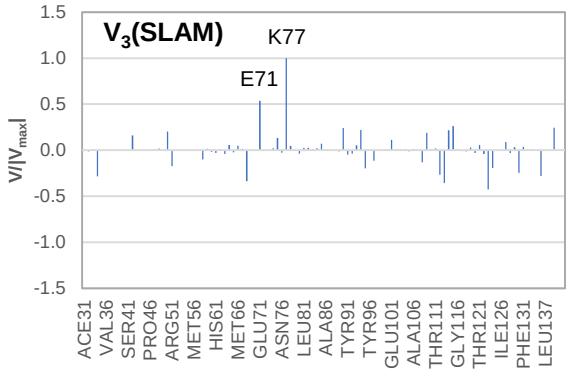
V3(SLAM)
K77
E71
V/|Vmax|
ACE31 VAL36 SER41 PRO46 ARG51 MET56 HIS61 MET66 GLU71 ASN76 LEU81 ALA86 TYR91 TYR96 GLU101 ALA106 THR111 GLY116 THR121 ILE126 PHE131 LEU137

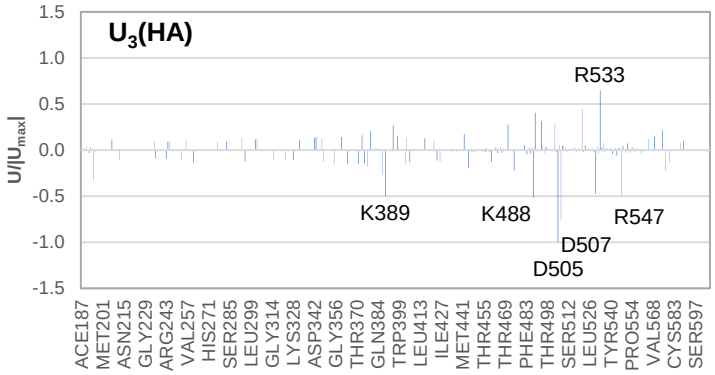
U3(HA)
R533
K389
K488
R547
D507
D505
U/|Umax|
ACE187 MET201 ASN215 GLY229 ARG243 VAL257 HIS271 SER285 LEU299 GLY314 LYS328 ASP342 GLY356 THR370 GLN384 TRP399 LEU413 ILE427 MET441 THR455 THR469 PHE483 THR498 SER512 LEU526 TYR540 PRO554 VAL568 CYS583 SER597

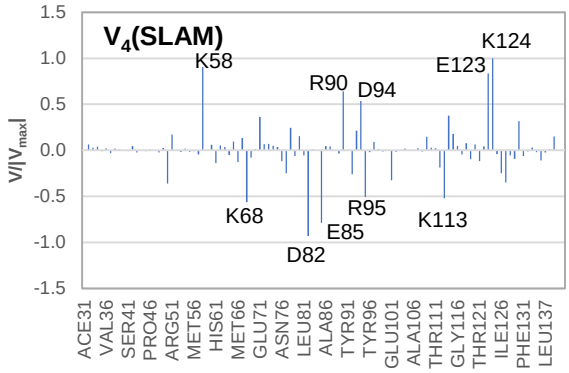
V4(SLAM)
K58
K124
E123
R90
D94
K68
R95
K113
E85
D82
V/|Vmax|
ACE31 VAL36 SER41 PRO46 ARG51 MET56 HIS61 MET66 GLU71 ASN76 LEU81 ALA86 TYR91 TYR96 GLU101 ALA106 THR111 GLY116 THR121 ILE126 PHE131 LEU137

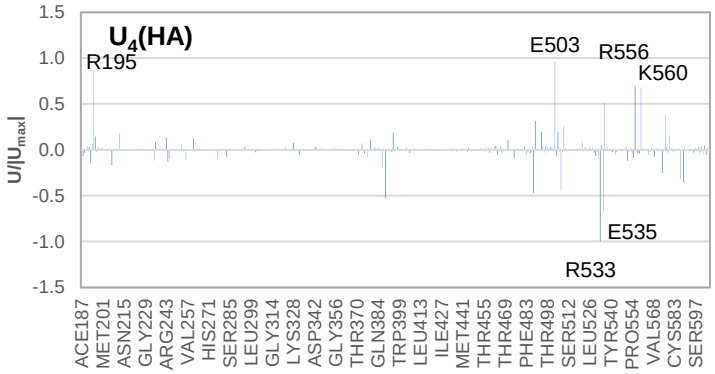
U4(HA)
R195
E503
R556
K560
E535
R533
U/|Umax|
ACE187 MET201 ASN215 GLY229 ARG243 VAL257 HIS271 SER285 LEU299 GLY314 LYS328 ASP342 GLY356 THR370 GLN384 TRP399 LEU413 ILE427 MET441 THR455 THR469 PHE483 THR498 SER512 LEU526 TYR540 PRO554 VAL568 CYS583 SER597

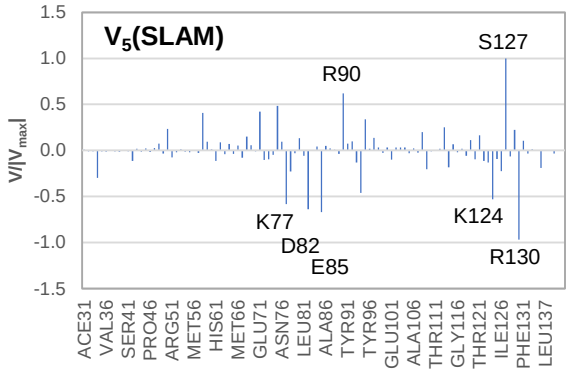
V5(SLAM)
S127
R90
K77
K124
D82
E85
R130
V/|Vmax|
ACE31 VAL36 SER41 PRO46 ARG51 MET56 HIS61 MET66 GLU71 ASN76 LEU81 ALA86 TYR91 TYR96 GLU101 ALA106 THR111 GLY116 THR121 ILE126 PHE131 LEU137

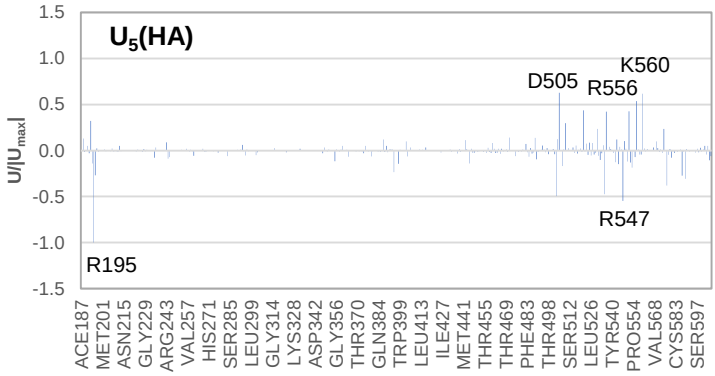
U5(HA)
K560
D505
R556
R547
R195
U/|Umax|
ACE187 MET201 ASN215 GLY229 ARG243 VAL257 HIS271 SER285 LEU299 GLY314 LYS328 ASP342 GLY356 THR370 GLN384 TRP399 LEU413 ILE427 MET441 THR455 THR469 PHE483 THR498 SER512 LEU526 TYR540 PRO554 VAL568 CYS583 SER597

Figure. S4 (continued)